



Long-term climatological trends driving the recent warming along the Angolan and Namibian coasts

Folly Serge Tomety¹ · Serena Illig^{1,2} · Marek Ostrowski^{1,3} · Founi Mesmin Awo¹ · Marie-Lou Bachèlery^{4,5} · Noel Keenlyside⁴ · Mathieu Rouault¹

Received: 26 February 2024 / Accepted: 3 June 2024
© The Author(s) 2024

Abstract

The coastal regions off Angola and Namibia are renowned for their highly productive marine ecosystems in the southeast Atlantic. In recent decades, these regions have undergone significant long-term changes. In this study, we investigate the variability of these long-term changes throughout the annual cycle and explore the underlying mechanisms using a 34-year (1982–2015) regional ocean model simulation. The results reveal a clear seasonal dependence of sea surface temperature (SST) trends along the Angolan and Namibian coasts, with alternating positive and negative trends. The long-term warming trend in the Angolan coastal region is mainly explained by a pronounced warming trend in the austral spring and summer (November–January), while the decadal trend off Namibia results from a counterbalance of an austral winter cooling trend and an austral summer warming trend. A heat budget analysis of the mixed-layer temperature variations shows that these changes are explained by a long-term modulation of the coastal currents. The Angolan warming trend is mainly explained by an intensification of the poleward coastal current, which transports more warm equatorial waters towards the Angolan coast. Off Namibia, the warming trend is attributed to a reduction in the northwestward Benguela Current, which advects cooler water from the south to the Namibian coast. These changes in the coastal current are associated with a modulation of the seasonal coastal trapped waves that are remotely-forced along the equatorial waveguide. These long-term changes may have significant implications for local ecosystems and fisheries.

Keywords Warming decadal trend · Seasonal variability · Coastal upwelling · Southeastern Atlantic · Heat budget analysis

In memory of our dear colleague, mentor and friend, Prof. Mathieu Rouault, who dedicated his life to the study and understanding of the air-sea interaction in the Benguela Upwelling System. His passion, dedication and invaluable contributions will always be remembered.

✉ Folly Serge Tomety
Serge.Tomety@uct.ac.za

- ¹ Department of Oceanography, Nansen Tutu Center, University of Cape Town, Rondebosch, Cape Town, South Africa
- ² Laboratoire d'Etudes en Géophysique et Océanographie Spatiale (LEGOS), CNRS/IRD/UT3/CNES, Toulouse, France
- ³ Institute of Marine Research and Bjerknes Centre for Climate Research, Bergen, Norway
- ⁴ Geophysical Institute, University of Bergen and Bjerknes Centre for Cate Research, Bergen, Norway
- ⁵ CMCC Foundation, Euro-Mediterranean Center on Climate Change, Bologna, Italy

1 Introduction

The Tropical Angola Upwelling System (TAUS) and North Benguela Upwelling System (NBUS) are among the most productive marine ecosystems in the southeastern Atlantic Ocean and represent a great source of food security and economic livelihoods for local communities (Hutchings et al. 2009; Sowman and Cardoso 2010). In both systems, coastal upwelling yields the rise of the thermocline, bringing cold deep nutrient-rich water to the euphotic zone, creating optimal conditions for the feeding and spawning of small pelagic fishes. However, these abundant fish resources are affected by ocean variability and climate change. Therefore, there is an urgent need to improve our understanding of the variability of the TAUS and NBUS, to describe the long-term changes they undergo, and to identify the underlying mechanisms and their potential impacts on the fisheries.

Both the TAUS and the NBUS exhibit lower Sea Surface Temperatures (SST) near the coast compared to those further

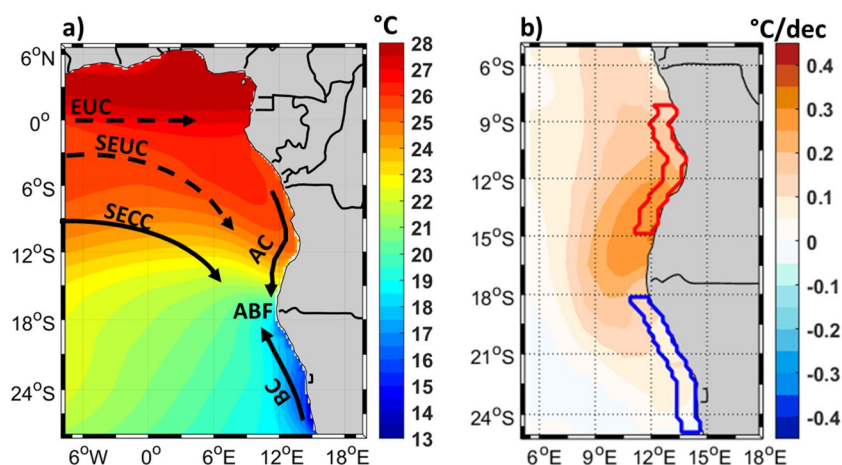


Fig. 1 **a** Mean sea surface temperature (SST, °C) and schematic of the circulation in the southeastern tropical Atlantic. Solid arrows indicate the surface currents, and the dashed arrow indicate the sub-surface current, composed of the Equatorial Under Current (EUC), the South Equatorial Under Current (SEUC), the South Equatorial Counter Current (SECC), the Angola Current (AC), and the Benguela Current (BC). **b** Long-term linear trend of SST in °C/decade (°C/

dec). The red and blue lines delineate the TAUS and NBUS coastal zones, respectively. Data come from the combination at $1^\circ \times 1^\circ$ of Optimum Interpolated SST $0.25^\circ \times 0.25^\circ$ (Huang et al. 2021), OISST $1^\circ \times 1^\circ$ (Reynolds et al. 2002) and Hadley SST (Rayner et al. 2003) from 1982 to 2015. The figure was created using the Matlab software (<https://mathworks.com>)

offshore (Awo et al. 2022; Körner et al. 2023). However, the surface waters of the TAUS are characterized by warm tropical conditions (Fig. 1a; Tchpalanga et al. 2018; Awo et al. 2022; Körner et al. 2023) and undergo a pronounced seasonal cycle, with the highest temperatures occurring in the austral autumn and the lowest temperatures in the winter (Awo et al. 2022; Körner et al. 2023). In contrast, the coastal surface waters of the NBUS remain relatively cold (Rouault 2012), such that the SST contrast between the coast and the open ocean ($> 3^\circ\text{C}$) is visible in satellite-derived data (Fig. 1a). This quasi-permanent coastal upwelling is driven by the prevailing alongshore equatorward surface wind, which intensifies from austral autumn to spring (Veitch et al. 2010). The strength of the upwelling varies along the Namibian coast and features several cells of cooler coastal SST (Fig. 1a; Shannon 1985; Chen et al. 2012; Bordbar et al. 2021). The circulation in NBUS is dominated by the cold alongshore equatorward Benguela Current, the eastern boundary current of the South Atlantic Gyre, driven by the southeasterly surface wind. Previous studies in the NBUS have reported a seasonal reversal of the current (equatorward in March–September and poleward in October–February, Mohrholz et al. 2008; Brandt et al. 2024), attributed to the seasonal changes in the local wind stress curl (Junker et al. 2015; Brandt et al. 2024).

The highly productive TAUS is sheltered from the eastern branch of the South Atlantic Anticyclone and is influenced by relatively weak coastal surface winds (Ostrowski et al. 2009; Blamey et al. 2015). It is driven by the poleward propagation of Coastal Trapped Waves (Tchpalanga et al. 2018; Awo et al. 2022; Körner et al. 2023) and mixing

induced by internal waves (Ostrowski et al. 2009; Tchpalanga et al. 2018; Zeng et al. 2021; Körner et al. 2023). Previous studies have described the passage of four Coastal Trapped Waves (CTWs) per year (Polo et al. 2008; Rouault 2012; Tchpalanga et al. 2018). Specifically, a first and a second downwelling CTW propagate along the Angolan coast in March and October, respectively, while a strong and a weaker upwelling CTW prevail in June–July and December–January, respectively. The circulation in the TAUS is dominated by the Angola Current (Fig. 1a), which transports warm equatorial water poleward along the Angolan continental slope and shelf (Kopte et al. 2017; Awo et al. 2022; Körner et al. 2023). Its intensity is modulated by the CTW (Bachélery et al. 2016; Illig et al. 2020), with downwelling waves favoring a stronger current. As a consequence, these warm waters reach the NBUS twice a year (in October and February) and have a substantial impact on fisheries in the region (Rouault 2012). The contrast between the warm Angola water and the cold Namibia water gives rise to a strong cross-frontal temperature gradient that delineates the two upwelling regions (Shannon 1985; Veitch et al. 2006; Rouault et al. 2018). Recent studies have investigated the factors responsible for the seasonal evolution of the SST in the southeastern Atlantic Ocean (Scannell and McPhaden 2018; Körner et al. 2023). Scannell and McPhaden (2018) analyzed the heat budget within the surface Mixed Layer (ML) from in situ observations recorded at the PIRATA buoy located at $[6^\circ\text{S}, 8^\circ\text{E}]$. Their results revealed that surface heat fluxes and vertical entrainment are the main contributors to the seasonal SST changes. Recently, Körner et al. (2023); (2024) demonstrated that the vertical mixing and

the upwelling induced by the CTW are the primary factors driving the upwelling in TAUS observed in austral winter. At the interannual timescale, the extreme warm and cold events off the coast of Angola and Namibia, the Benguela Niños/Niñas, constitute the main mode of interannual variability in SST (Florenchie et al. 2003; Rouault et al. 2018) and can have severe impacts on local fisheries (Binet et al. 2001; Boyer et al. 2001) and precipitations over southwestern Africa (Rouault et al. 2003; Lutz et al. 2015).

At the decadal scale, the coastal areas off Angola and Namibia exhibits a warming trend of up to 0.4 °C/decade (°C/dec) was observed between 1982 and 2015, with slightly lower values in the Namibian region (see Fig. 1b). Despite these notable trends, these regions have received limited attention. This may be attributed to a scarcity of long-term observational data and the challenge for models to properly simulate the Angola-Namibia region. Both coupled and uncoupled ocean models are known to suffer from a warm coastal bias due to poor clouds representation (Huang et al. 2007), atmospheric moisture bias (Hourdin et al. 2015; Deppenmeier et al. 2020), and errors in the coastal wind forcing (Koseki et al. 2018; Voldoire et al. 2019; Richter and Tokinaga 2020; Kurian et al. 2021). While a few studies acknowledge a significant warming of the coastal ocean fringe off Angola over the last decade (Vizy and Cook 2016; Vizy et al. 2018), the situation in the Namibian region remains a topic of debate. For example, Vizy and Cook (2016) used several reanalysis data to show that the SST along the Angolan and northern Namibian coasts exhibit a statistically significant warming trend, attributing it to the net downward atmospheric heat flux. More recently, Vizy et al. (2018) investigated the mechanisms driving the annual decadal change within the Angola-Namibia coastal region using a regional atmospheric model coupled with an intermediate-level ML ocean model. Their results indicate a warming trend along the Angolan coast (6°S–17°S) and a cooling trend along the Namibian coast (17°S–25°S). They suggest that the warming trend in the Angolan region is mainly associated with a weakening of the vertical entrainment, leading to less cooling of the surface water. Meanwhile, the cooling trend in the Namibian region would be associated with an intensification of the horizontal advection, bringing cooler water from the Benguela Current.

The few studies on long-term changes have focused on the annual trends, neglecting the examination of climatological trends. However, in the Angola-Namibia coastal region, especially off Angola, the annual cycle of SST is very strong, with different mechanisms at work. This raises the question of whether the decadal annual trends depicted in Fig. 1b and by Vizy and Cook (2016), and Vizy et al. (2018) remain constant during the upwelling and non-upwelling seasons, especially along the 1°-wide coastal band, which would imply distinct consequences for the ecosystems. In particular, the reproductive success of fish is critically dependent on environmental conditions during early life stages (Hjort 1914), and in the face

of decadal warming, one would expect a detrimental effect on the ecosystem. For example, in the case of *Sardinella aurita*, a small pelagic fish essential for the food security in Angola and well known to be highly sensitive to climatic stress (Cury and Roy 1989; Binet et al. 2001; Sabatés et al. 2006), such a critical period is concentrated only during the upwelling seasons. In this context, this study aims to investigate the decadal linear trend in the TAUS and NBUS in different seasons and to identify the processes responsible for these changes. For this purpose, we analyze the outputs of a surface ML heat budget from a 34-year long ocean model simulation of the tropical Atlantic. The paper is structured as follows: Section 2 outlines the material and methods, followed by the presentation of results in Section 3 and concluding remarks and discussion in Section 4.

2 Materials and methods

Our study mainly relies on the analysis of linear trends of the surface Mixed Layer Temperature (MLT) from observations and a regional simulation of the tropical Atlantic from 1982 to 2015.

2.1 Observed SST datasets

The observed linear trends over the period 1982–2015 are estimated from the weekly and daily Optimum Interpolation satellite-derived SST data (Reynolds et al. 2002; Huang et al. 2021) at 1°×1° and 0.25°×0.25° spatial resolution, respectively, and the 1°×1° Hadley SST data (Rayner et al. 2003). Using these three observational products, a combined data set is generated in order to reduce the discrepancies between the data products and to minimize the uncertainties associated with the decadal trend estimates. To derive the long-term trend map (Fig. 1), we first interpolate the 0.25°×0.25°-resolution OISST data onto the coarser 1°×1° grid of the lower-resolution observations using an averaging method and then compute the ensemble mean of the three datasets. To estimate the observed decadal trend off southwest Africa (Fig. 3a, b), the coastal SSTs within the 1°-wide coastal band are first estimated separately for each dataset. Low-resolution estimates are then meridionally interpolated every 0.25° and three coastal products are then combined into an ensemble-mean observational dataset. It is noteworthy that, the general spatiotemporal patterns in the decadal trend depicted in Fig. 1b and Fig. 3a, b from our composite observations are consistent across all three individual observational products analyzed separately (see Supplementary Material).

2.2 Tropical Atlantic Model configuration

The Coastal and Regional Ocean COmmunity model (CROCO, Shchepetkin and McWilliams 2005; Penven et al.

2006; Debreu et al. 2012) was used to produce a multi-decadal (1982–2015) simulation of the tropical Atlantic. We use the realistic simulation (named CROCO^{LONG}) developed in Illig et al. (2020) that extends from the Americas to Africa (62.25°W–17.25°E) from 30°S to 10°N, with a horizontal resolution of 1/12° and 37 terrain-following vertical levels stretched near the surface. The bathymetry is derived from the GEBCO_08 30" elevation database (<http://www.gebco.net>). Initial and northern/southern open lateral boundary conditions are estimated from the CARS2009 climatology (Ridgway et al. 2002; Dunn 2009). Boundary conditions are integrated using a mixed radiation-nudging scheme (Marchesiello et al. 2001). The model is forced by momentum, heat, and freshwater fluxes derived using bulk formulae (Kondo 1975) based on the daily-averaged surface fields at 0.7°×0.7° resolution from the DRAKKAR Forcing Set v5.2 (DFS; Dussin et al. 2016). The MLD is provided by the turbulent mixing scheme (K-profile parameterization; Large et al. 1994). An analytical diurnal cycle modulates the shortwave radiation. River runoffs are not included in the simulation, instead the sea surface salinity is restored to the CARS2009 climatological values. This configuration has been successfully used to study the coastal dynamics off southwest Africa on seasonal (Körner et al. 2024) and interannual (Illig et al. 2020) timescales. Comparisons with observations can be found in Illig et al. (2020).

2.3 Heat-budget within the mixed-layer

To diagnose the processes responsible for the surface temperature decadal changes, the heat budget within the time-varying Mixed Layer (ML) is computed online by the model at each time step during the simulation as in (Illig et al. 2014). This ensures that the heat budget is closed, takes transients into account, avoiding errors associated with nonlinearities. The Mixed Layer Depth (MLD, h) is determined by the turbulent mixing K-Profile parametrization (Large et al. 1994). The rate of change of the mixed-layer temperature (ΔT) is driven by the advection (**X-ADV**, **Y-ADV**, **Z-ADV**), the vertical mixing (**V-MIX**: sum of vertical diffusivity at the base of the ML (**DIFF**) and entrainment (**ENTR**)), and the forcing by the surface heat fluxes (**SFORC**) tendencies, such that:

$$\underbrace{\partial_t \langle T \rangle}_{\Delta T} = - \underbrace{\langle u \partial_x T \rangle}_{\text{X-ADV}} - \underbrace{\langle v \partial_y T \rangle}_{\text{Y-ADV}} - \underbrace{\langle w \partial_z T \rangle}_{\text{Z-ADV}} - \underbrace{\frac{1}{h} (k_z \partial_z T)_{z=-h}}_{\text{DIFF}} - \underbrace{\frac{1}{h} \partial_t h \times (\langle T \rangle - T_{z=-h})}_{\text{ENTR}} + \underbrace{\frac{Q^* + Q_S - Q_P}{\rho C_p h}}_{\text{SFORC}} \quad (1)$$

where T is the model potential temperature; (u , v , w) are the components of the ocean currents; k_z is the vertical diffusion coefficient; Q_S is the net surface solar heat flux, and Q_P is the fraction of solar radiation that penetrates below the base of the MLD; Q^* includes the surface longwave radiations, and latent, and sensible heat fluxes. Brackets denote the vertical average over the MLD: $\langle T \rangle = \frac{1}{h} \int_{-h}^0 T dz$. Note that the **ENTR** term is not explicitly calculated online but it closes the ML budget and therefore also includes numerical diffusions associated with the temporal scheme. Because of the implicit diffusion in the upstream advection scheme, explicit lateral diffusion is set to zero.

The model timestep is 600 s. We store 3-day averages of the state variables and surface fluxes, along with daily averages of the ML heat budget tendencies. In the following, we assume that, in terms of monthly means, the instantaneous temperature at midnight, reconstructed using the summed-up contribution of the daily tendencies, is not different from the daily averaged temperature.

2.4 Estimation of the linear trends

Observed and modeled linear trends are calculated using a classical linear least squares regression method. For the 1°-wide coastal band along the southwest African coast, we estimate the MLT Long-term Decadal Trends (LDT) over the period 1982–2015 and also compute the MLT decadal trends for each calendar month, referred to as Monthly climatological Decadal Trends (MDT). Statistical significance is estimated using the non-parametric Mann-Kendall and seasonal Kendall tests (Mann 1945; Kendall 1948). The results, presented in Fig. 3, show that the modeled LDT and MDT are in good agreement with the observations (see Section 3.1). This gives confidence in the estimation and analysis of the processes driving these changes.

As warned by Alory and Meyers (2009), it is important to exercise caution when determining the linear trends of the heat budget tendencies for estimating their contributions to the linear trend of the MLT. This is illustrated in Fig. 2a, b, using the **YADV** tendency term averaged in the TAUS. First, it is important to acknowledge that the LDT of the tendency terms (red line in Fig. 2a) are second-order derivatives that reflect an acceleration or deceleration of the linear temperature evolution (red lines in Fig. 2b). This means that the LDT of a tendency term describes an increase or decrease in the MLT LDT over the period considered, rather than the linear change itself. For instance, in Fig. 2b, the linear trend decreases over time, associated with a negative slope in the tendency (Fig. 2a). Consequently, such a method is not fully suitable for identifying the processes responsible for the MLT LDT. Instead, one may consider estimating the mean of the heat-budget tendencies (blue line in Fig. 2a). However, the resulting rate of change would only represent

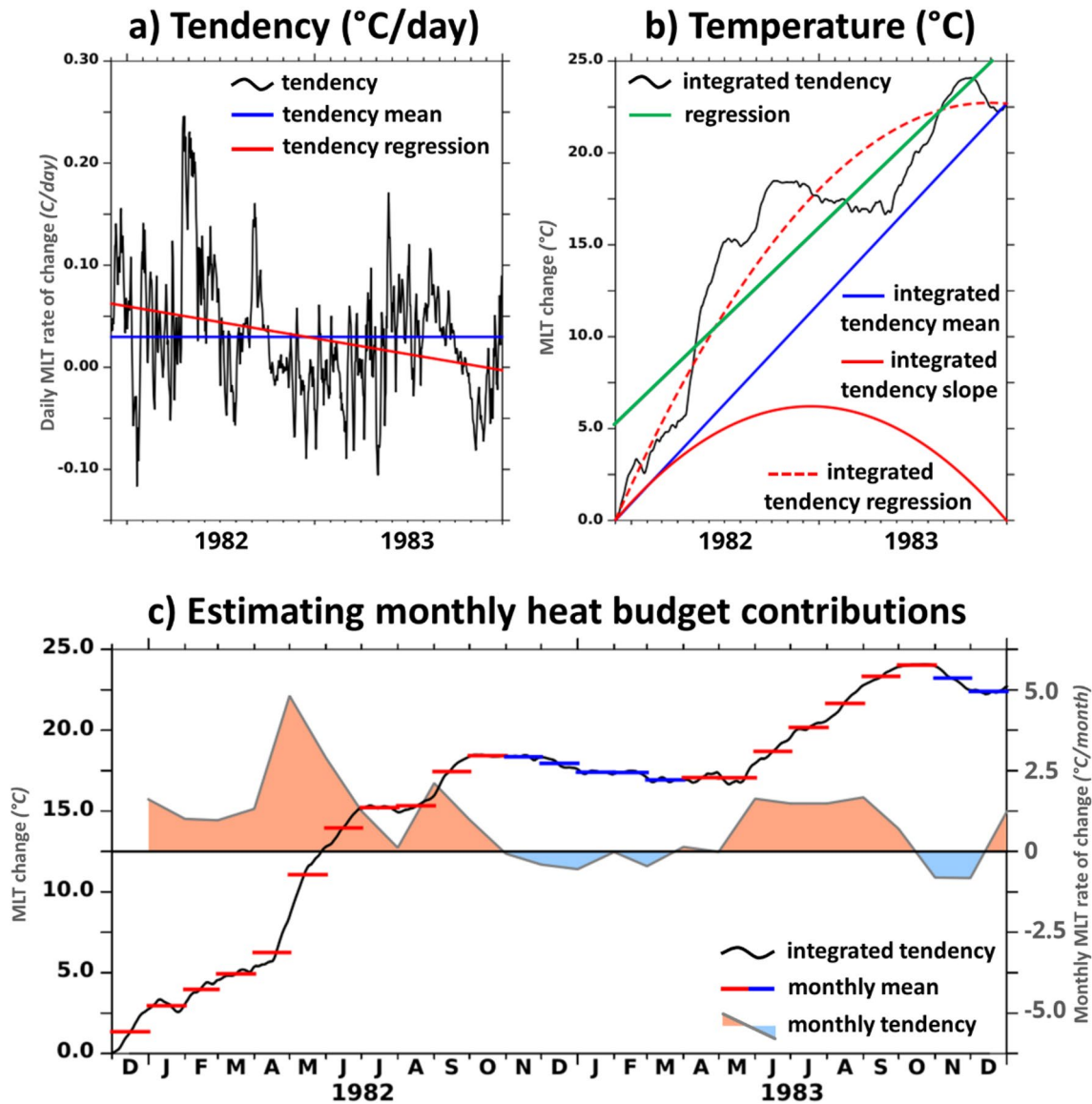


Fig. 2 Analyzing the decadal changes in the heat budget tendency terms, using the example of the **YADV** tendency averaged over the TAUS (15°S–8°S) within the 1°-wide coastal band from December 1981 to December 1983. **a** The black line displays the daily tendency (°C/day), and the blue and red lines depict the time-averaged ($y = b$) and linear regression ($y = a \times t + b$) of the tendency term, respectively. **b** MLT evolution associated with the tendency term. The black line is the integration over time of the tendency term (in °C), and the blue and red lines are the integration over time of the mean tendency ($\int b \cdot dt$) and the tendency trend ($\int (a \times t) \cdot dt$), respectively. The dashed red line is the integration over time of the linear regres-

sion of the tendency term ($\int (a \times t + b) \cdot dt$). The green line shows the linear regression of the reconstructed temperature variations. **c** Methodology used to estimate monthly heat budget contribution to the MLT variations. The black line shows the temperature variations (°C) from the integration of the daily tendency. The steps are the monthly means (°C), in red (blue) when the monthly value is higher (lower) than the previous month. The gray curve with light blue and orange shading represents the monthly rate of change (°C/month) estimated as the difference between two consecutive monthly averages. The figure was created using the PyFerret program (<http://ferret.pmel.noaa.gov/Ferret/>)

the slope between the start and end points of the integrated timeseries (blue line in Fig. 2b) and would therefore be heavily influenced by seasonal, intraseasonal, and interannual variability. It is preferable to reconstruct the temperature variations associated with each process controlling the MLT variations by integrating the heat budget tendencies from

Eq. 1 over time and then estimating the slope that best fits this timeseries (green line in Fig. 2b). However, the LDT obtained would need to be compared to a reference simulation or period that does not exhibit any decadal trend in the MLT. Conversely, from a climatological perspective, the seasonal variations dominate the coastal MLT variability in

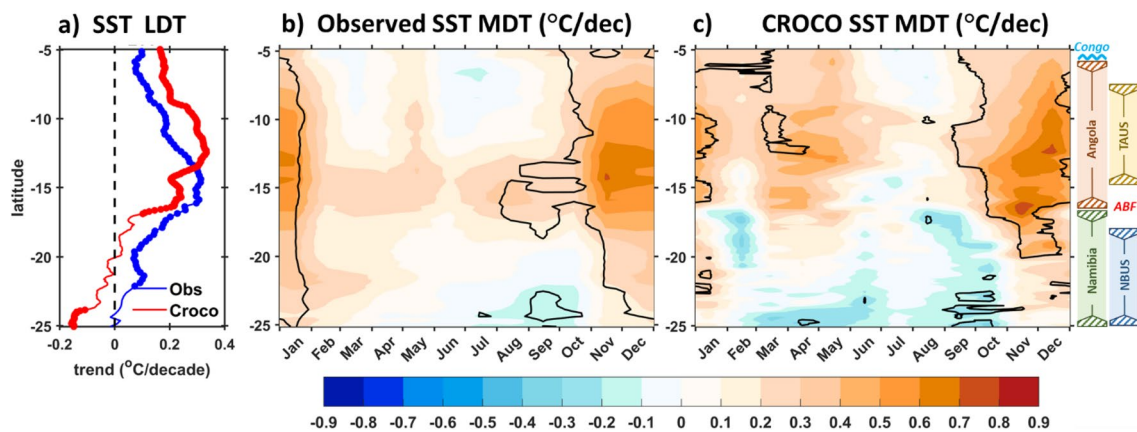


Fig. 3 Linear trend (in $^{\circ}\text{C}/\text{dec}$) of the SST averaged within the 1° -wide coastal fringe along the Angola-Namibia coast over the period 1982–2015. **a** Annual long-term trends of observed (blue) and modeled (CROCO, red) SST. **b**, **c** Hovmöller diagrams of the

monthly climatological decadal linear SST trends for the observations and CROCO, respectively. Dashed contours indicate statistically significant values at the 95% confidence level. The figure was created using the Matlab software (<https://mathworks.com>)

the TAUS and NBUS. Thus, every year the MLT and the heat budget terms undergo pronounced and systematic trends during each calendar month, triggering seasonal warming and cooling phases. Our objective is to analyze the decadal changes in these monthly MLT rates of change, which induce an alteration of the MLT seasonal cycle, associated with changes in the balance of the processes. As a concrete example, one could consider the effect of the seasonal passage of the downwelling CTW off Angola in September. It causes a seasonal warming phase associated with a poleward flow of the Angolan current and thus a positive **Y-ADV**. If this seasonal remote wave increases with time due to changes in the equatorial basin, then we would observe a positive trend in the **Y-ADV** tendency during this season, which would explain an increased warming during the warming phase of the seasonal cycle. The calculation of the MDT of the MLT and tendency terms allows the estimation of decadal changes in the seasonal cycle and the identification of the processes driving these changes. On the seasonal scale, we assume that each year is independent of the others. This implies that the MDT of the heat budget contributions reflect the linear increase or decrease in the MLT of a given month, rather than a quadratic one.

To analyze the MDT, we employ an adapted methodology to examine the processes driving the climatological changes in the MLT decadal trend using the ML heat budget outputs from CROCO. We first reconstruct the temperature evolution associated with each process controlling the MLT variations by integrating the daily heat budget tendencies from Eq. 1 over time and then compute monthly means. The monthly rates of change associated with each process are then calculated by taking the difference between two consecutive monthly means. This is illustrated in Fig. 2c, for the **YADV** contribution in the TAUS. The black curve

shows the integrated temperature changes from December 1, 1981, with the steps representing monthly means, and the gray curve is the monthly rate of change. Thereafter, the climatology of this monthly heat budget enables to recall the phenology of the dominant processes driving the MLT changes from one season to another and to verify that the model is realistic (see Section 3.2). The analysis of the decadal changes of the monthly heat budget tendencies allows to identify the processes responsible for the long-term evolution of the MLT at a given season (see Sections 3.3 et 3.4).

3 Results

3.1 Long-term and climatological SST decadal trends

Figure 3 shows the observed and modeled long-term trends in SST at both annual (Fig. 3a) and seasonal (Fig. 3b, c) scales. In agreement with, Vizy and Cook (2016) and Vizy et al. (2018), the observations exhibit a mean warming trend larger than 0.1°C per decade ($^{\circ}\text{C}/\text{dec}$) along most parts of the Angolan and Namibian coasts (see blue curve in Fig. 3a). The southern Angola, between 12°S and 17°S , undergoes the largest warming trend over the 1982–2015 period ($> 0.25^{\circ}\text{C}/\text{dec}$). The southern Namibian coastal region (22°S – 25°S) only shows a weak warming trend of less than $0.05^{\circ}\text{C}/\text{dec}$.

At the seasonal scale (Fig. 3b), the observed SST trend along the Angolan and Namibian coasts exhibits a clear seasonal dependence with alternating positive and negative trends. Our observational dataset highlights a statistically significant warming trend during the austral spring and summer (September–January), with a peak exceeding $0.8^{\circ}\text{C}/\text{dec}$ at 14°S in November–December in the ABF. In contrast,

the rest of the year experiences a moderate coastal cooling trend of up to -0.2 °C/dec, except in the ABF zone where a warming trend persists throughout the year. Along the coasts of Angola, the pronounced warming trend in austral spring/summer underlies the overall annual warming trend reflected in the annual observed SST trend (Fig. 3a). Contrastingly, south of 19°S , the counterbalance of the austral winter cooling trend and the spring/summer warming trend in the southern Namibian coastal zone results in the very weak annual trend of the observed SST.

A comparison between the SST long-term trend in CROCO and in the observations (Fig. 3a) reveals that CROCO reproduces well the annual warming trend in the Angolan and North Namibian coastal region (North of 20°S) with a maximum value of $+0.33$ °C/dec at 13°S . However, the model fails to capture the weak positive trend along the south Namibian coast, instead showing a cooling trend up to -0.16 °C/dec south of 20°S , in agreement with Vizzy et al. (2018). On a seasonal scale (Fig. 3c), the model successfully reproduces the strong warming trend in the austral spring/summer and the cooling trend in the winter along both the Angolan and the Namibian coasts. However, CROCO overestimates the warming trend in March–April off Angolan and the cooling trend in the Namibian coastal region. This results in an overall annual cooling trend in the model south of 20°S (Fig. 3a). Possible explanations for this bias in the model include unrealistic acceleration trends in equatorward coastal winds, which would lead to excessive upwelling and evaporation, and to stronger equatorward horizontal currents advecting cold water northward. These discrepancies between model and observations can also be attributed to the coarse resolution of satellite data, which struggles to accurately capture the coastal upwelling (García-Reyes et al. 2015; Carr et al. 2021). Despite these differences, the good agreement between the modeled and observed SST trends at the seasonal scale gives confidence to use the CROCO outputs to unravel the mechanism responsible for the decadal climatological changes in SST observed along the Angolan and Namibian coasts. This is done in the following sections.

3.2 Climatological heat budget within the mixed layer

To comprehensively analyze the climatological trends in the MLT within both the TAUS and the NBUS, it is important to first examine the seasonal dynamics of the MLT in each region. In the TAUS (8°S – 15°S , Fig. 4a), the MLT exhibits a pronounced seasonal cycle, characterized by high temperatures above 25 °C during the austral summer and autumn months, peaking in March (~ 28 °C). The austral winter season is characterized by lower temperatures, dropping below 24 °C and reaching a minimum of 21 °C in August. Consequently, the MLT undergoes a cooling phase from

March to August, followed by a warming phase during the rest of the year. Notably, the austral winter period, known as the upwelling season in the TAUS, is under the influence of relatively weak surface winds, with a wind stress amplitude lower than 0.03 N.m^{-2} (Fig. 4a; Ostrowski et al. 2009; Blamey et al. 2015). Contrastingly, the surface waters in the NBUS (18°S – 25°S , Fig. 4b) are relatively cold. The MLT ranges between 13.5 °C and 19 °C, with the lowest temperature observed in austral winter and the highest in austral autumn. Consequently, similar to the TAUS, the surface ML of the NBUS cools between March and August and warms during the rest of the year (Fig. 4b). In addition, the wind stress amplitude in the NBUS remains above 0.075 N.m^{-2} throughout the year, with the highest values observed in austral spring (Fig. 4b). Consequently, the relatively lower temperatures in the NBUS can be attributed to the quasi-permanent wind-driven upwelling in the region (Fig. 4b; Veitch et al. 2010), while in the TAUS the seasonal variability of the MLT is not driven by the modulation of the surface winds but rather by the passage of equatorially forced annual and semi-annual CTWs (Körner et al. 2023, 2024).

The analysis of the ML heat budget reveals that the surface forcing contribution (**SFORC**, see Eq. 1) consistently warms the coastal ocean waters off Namibia and Angola throughout the year (Fig. 4c, d), in agreement with Körner et al. (2023) and Vizzy et al. (2018). This highlights the dominance of solar fluxes over non-solar fluxes in both regions. The vertical mixing contribution (**V-MIX**, see Eq. 1) plays a crucial role in cooling the coastal ocean waters off Angola and Namibia throughout the year. Indeed, it diffuses the surface heat content downward beneath the ML and thus closely counterbalances the externally forced surface warming (**SFORC**), especially during austral winter. The residual, resulting from the summation of the **SFORC** and **V-MIX**, still warms the coastal ocean waters of Namibia and Angola and varies between 0 – 3 °C/month and 0 – 6 °C/month in the TAUS and NBUS, respectively.

On average, within the 1° -wide coastal band along the NBUS, the horizontal advection (**Hor-ADV**), dominated by the zonal advection (**X-ADV**, Fig. 4f), cools the ocean waters throughout the year, with stronger effect in the austral summer and weaker in winter. In contrast, in the TAUS, the **Hor-ADV** (Fig. 4e) alternates between positive and negative values, sequentially warming and cooling the coastal ML at semi-annual frequencies in agreement with the passage of downwelling and upwelling equatorially-forced CTWs that can be depicted on the variations of the Sea Surface Height Anomalies (SSHA, Fig. 4a). Notably, **Hor-ADV**, dominated by the **Y-ADV**, warms the ML in January–February and August to October, with a maximum value exceeding 1.5 °C/month in August–September.

The coastal upwelling dynamics, bringing deep cold water towards the surface, also contributes to the cooling of the Angolan and Namibian coastal surface waters. It is

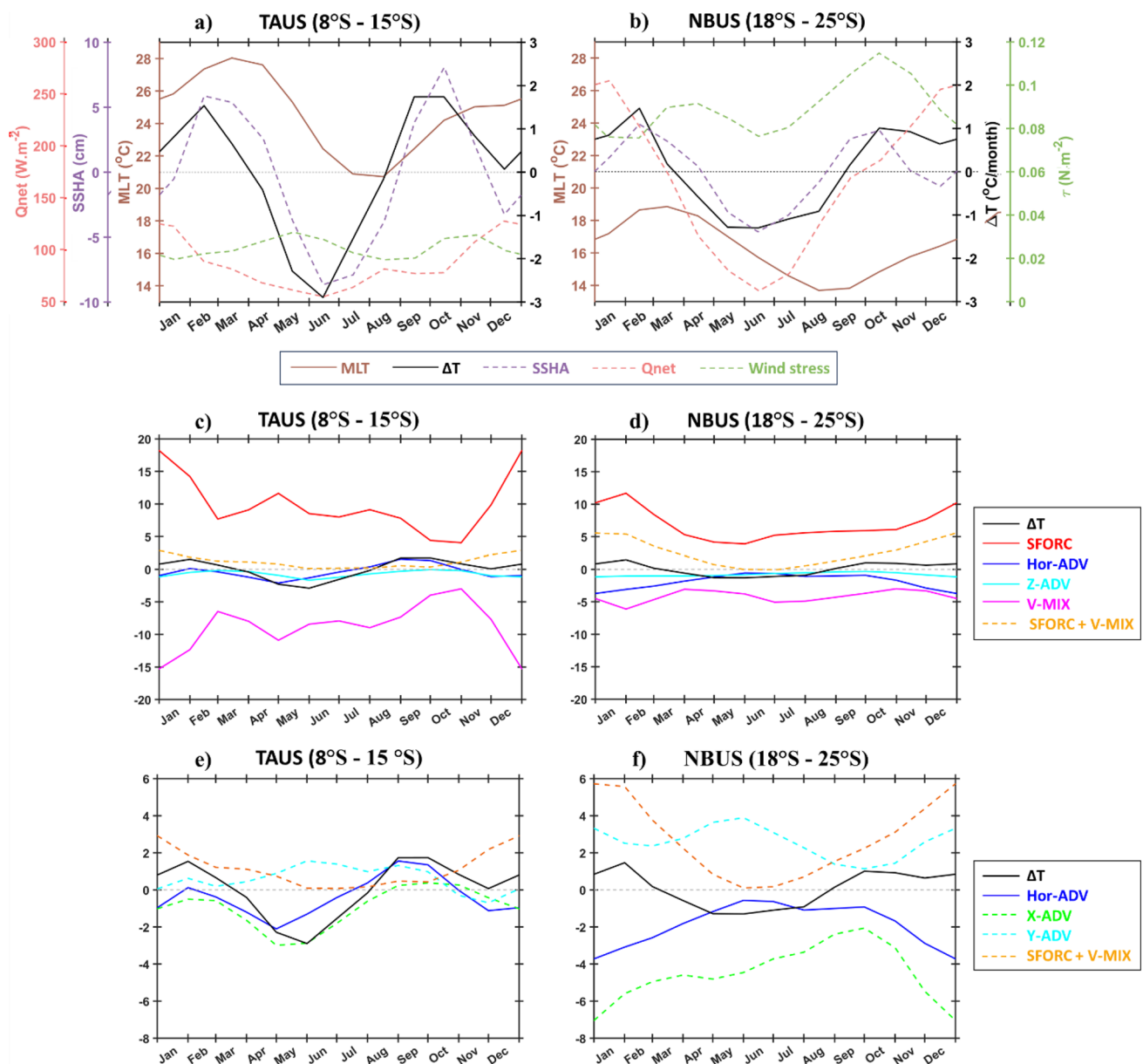


Fig. 4 Climatological conditions (1982–2015) in the 1°-wide coastal fringe in the TAUS (8°S–15°S, left panels) and in the NBUS (18°S–25°S, right panels). **a, b** display the climatology of the MLT (brown solid line, °C), the monthly rate of temperature change (ΔT , black solid line, °C/month), the SSH anomaly (purple dashed line, cm), the net surface heat flux (Q_{net} , light coral dashed line, $W.m^{-2}$), and the wind stress amplitude (green dashed lines, $N.m^{-2}$). **c, d** show

the climatology of the ML budget terms (°C/month), with the surface heat forcing in red, the horizontal advection in blue, the vertical mixing in magenta, and the vertical advection in cyan. **e, f** show the decomposition of the climatological horizontal advection into its zonal (dashed green line) and meridional (dashed cyan line) components. The figure was created using the Matlab software (<https://mathworks.com>)

characterized by negative vertical advection contribution (**Z-ADV**) in both regions throughout the year, exhibiting clear seasonal variations. In the TAUS, the cooling effect of the **Z-ADV** (Fig. 4c) is more pronounced in the austral winter (May–July) and summer (December–January), coinciding with the passage of the equatorially-forced upwelling CTW associated with negative SSHA (see Fig. 3a Sea Surface

Height Anomaly (SSHA); Ostrowski et al. 2009; Kopte et al. 2017; Tchpalanga et al. 2018). In the austral spring (September–October) and late summer (February–March), the **Z-ADV** term weakens significantly, and approaches zero, associated with the passage of the equatorially-forced downwelling CTW (Fig. 4a). In the NBUS, the cooling effect of the **Z-ADV** (Fig. 4d) is stronger in austral summer and

weaker in late austral winter, consistent with the seasonal modulation of the coastal equatorward wind (Fig. 4b).

In summary, the ML in the TAUS and NBUS cools in late autumn and winter and warms during the rest of the year. The cooling is mainly associated with the combination of **Z-ADV** and **Hor-ADV**. The subsurface forcing **V-MIX** also cools the TAUS and NBUS at that period but is the mirror effect of the atmospheric forcing **SFORC**. The warming of the ML in the TAUS and NBUS is primarily associated with **SFORC**. However, in spring, **Hor-ADV** contributes also to the warming of the ML in the TAUS. Our results are in agreement with (Körner et al. 2023), which underscores that the CROCO simulation realistically captures the ML dynamics of the Angola-Namibia region. In the following section, we analyze the

decadal climatological trend in the coastal MLT and the processes underlying these trends.

3.3 Decadal climatological changes in the mixed layer

Here, we first analyze the monthly climatological decadal trend (MDT) of the temperature averaged within the ML. As expected, the MDT of the MLT (Fig. 5a) displays a very similar seasonality to that of the SST shown in Fig. 3c, with a statistically significant warming trend along Angola-Namibia in the austral spring/summer (September to January), which is stronger in the TAUS (above $0.6\text{ }^{\circ}\text{C}/\text{dec}$ in December, Fig. 5c) than in the NBUS ($\sim 0.2^{\circ}\text{C}/\text{dec}$, Fig. 5d). During the rest of the year, the NBUS undergoes a moderate

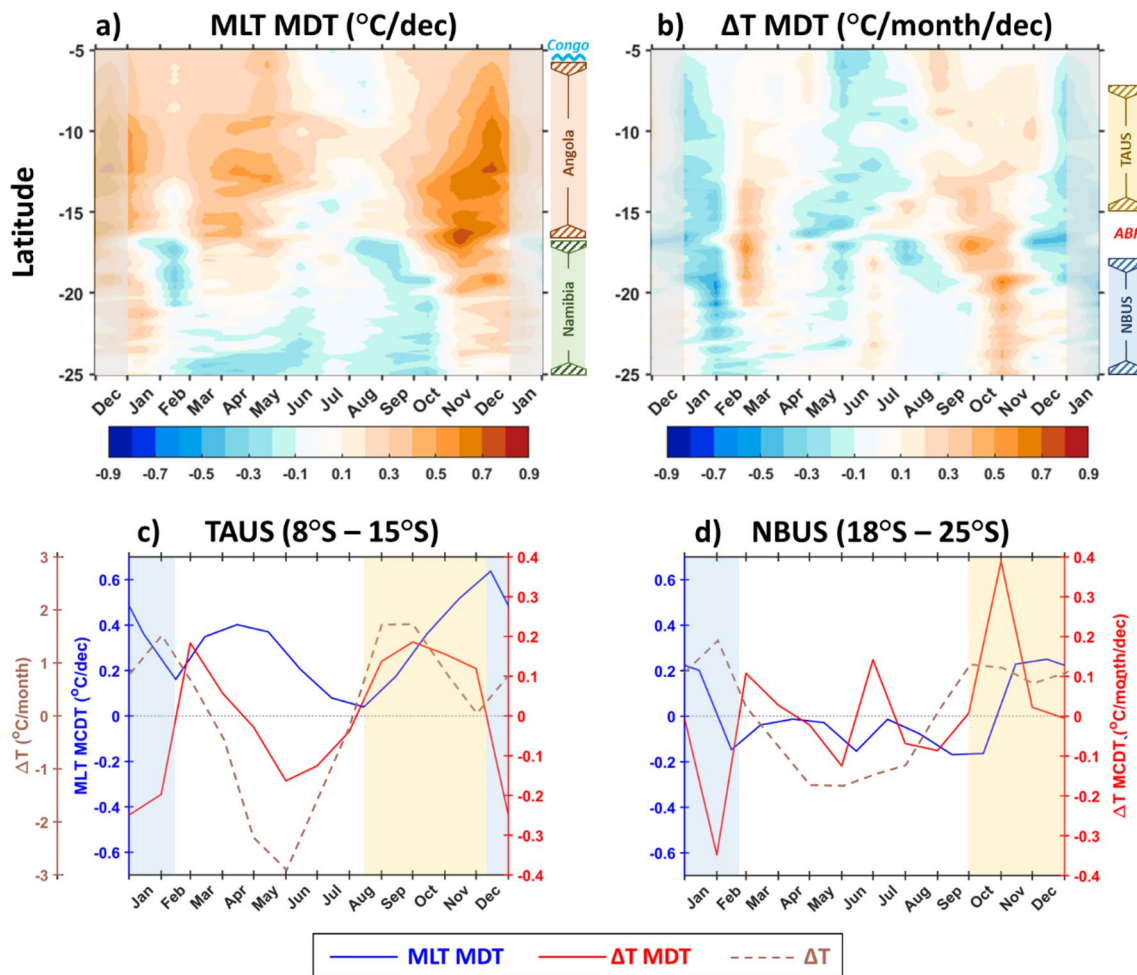


Fig. 5 Top panels show latitude-time Hovmöller diagrams of the monthly climatological decadal linear trends of **a** the MLT ($^{\circ}\text{C}/\text{dec}$) and **b** the summed-up contribution of all the processes driving the MLT changes (ΔT , $^{\circ}\text{C}/\text{month}/\text{dec}$). Grey shading denotes an extension of the climatology period. Bottom panels display MLT MDT (blue line, $^{\circ}\text{C}/\text{dec}$) and ΔT MDT (red line, $^{\circ}\text{C}/\text{month}/\text{dec}$), along

with climatological ΔT (dashed brown line, $^{\circ}\text{C}/\text{month}$, from Fig. 4) averaged in the TAUS (**c**, [$8^{\circ}\text{S}-15^{\circ}\text{S}$] 1° -wide coastal band) and in the NBUS (**d**, [$18^{\circ}\text{S}-25^{\circ}\text{S}$] 1° -wide coastal band). Yellow and blue shadings highlight focus periods of warming and cooling decadal trends, respectively. The figure was created using the Matlab software (<https://mathworks.com>)

cooling trend, while the TAUS shows a secondary warming trend in the austral autumn (~ 0.4 °C/dec).

It is important to acknowledge that the MLT MDT exhibits a marked seasonal cycle in both the TAUS and NBUS, undergoing null or quasi null decadal trend during periods characterized by substantial seasonal temperature variations (Fig. 5c, d). For instance, in the TAUS (Fig. 5c), negligible decadal changes (MLT MDT, blue line) are reported in August during the seasonal warming of the coastal ML (ΔT , dashed brown line). Consequently, at seasonal scale, the MLT decadal trend of a particular calendar month is not the result of the integration of the MLT rate of changes over an extensive period of time. For instance, the positive linear MDT observed along the Angolan-Namibian coasts in November-December can be attributed to a decadal warming trend occurring only few months before and that amplifies year after year. As a result, the integration over time of MDT heat budget contributions does not reflect the acceleration/deceleration of MLT changes but rather the linear climatological changes, as assumed in Section 2.4.

In order to validate this methodology, we first analyze the MDT of the summed-up contribution of all the terms driving the MLT changes (ΔT , see Eq. 1). As shown in Fig. 5b, the linear MDT of ΔT shows alternating positive and negative trends. In the Angolan region, ΔT MDT undergoes a semiannual cycle that explains the monthly climatological decadal variations of the MLT (Fig. 5a). ΔT MDT increases up to $+0.3$ °C/month/dec in the austral spring and starts to decrease in December, marking the seasonal maximum of the MLT MDT. ΔT MDT then increases again in early autumn (~ 0.15 °C/month/dec), marking the seasonal attenuation of the positive MLT MDT. In the TAUS coastal band (1° -wide within 8°S - 15°S , Fig. 5c), the MLT experiences a seasonal warming in austral spring (positive climatological ΔT in August-November) and therefore the positive ΔT MDT in spring ($\sim +0.2$ °C/month/dec) indicates an increase in the rate of the seasonal warming. Similarly, in austral summer, the MLT seasonally warms (positive ΔT in December-February), so the negative summer ΔT MDT (~ -0.25 °C/month/dec) indicates a gradual decreased warming rate. In austral winter, the MLT is cooling (negative ΔT in April-July), hence the negative winter ΔT MDT (~ -0.17 °C/month/dec) indicates an increasing cooling rate.

Along the Namibian coast, ΔT undergoes similar MDTs to those observed in the Angolan domain (Fig. 5b). ΔT increases by up to $+0.5$ °C/month/dec in austral spring (October-November) and decreases by up to -0.6 °C/month/dec in austral summer (January-February). In early austral autumn (February-April) and winter (June-July), ΔT increases slightly up to $+0.3$ °C/month/dec and $+0.2$ °C/month/dec respectively, while in late austral autumn (May-June) and late winter (August-September), ΔT decreases slightly up to -0.2 °C/month/dec and -0.1 °C/month/dec

respectively. In the NBUS coastal band (1° -wide within 18°S - 25°S , Fig. 5d), the significant positive MDT in austral spring and the significant negative trend of ΔT in summer correspond to the decadal warming of the MLT in austral summer and its decadal cooling during the rest of the year. The slightly alternating negative and positive trend from autumn to winter is due to fluctuations during the decadal cooling of the MLT. In late austral spring and early summer (October-January), the MLT is seasonally warming (positive ΔT in Fig. 5d), and this warming has increased up to $+0.4$ °C/month/dec during the last three decades, accounting for the warming trend in NBUS observed in the austral summer (Fig. 3b).

In conclusion, the MDT of ΔT in the Angola-Namibia coastal regions is in quadrature with the trend of MLT in the region. This validates the methodology employed and opens the possibility to analyze the processes driving the observed MDT.

3.4 Processes driving the MLT trend

In this section, we examine the potential drivers of the decadal climatological trend of the MLT. We analyze the MDT of each term of the monthly ML heat budget, first in the TAUS (Fig. 6) and then in the NBUS (Fig. 7), in order to explain the ΔT MDT.

As described in the previous section, the MDT of the summed-up contribution of all processes (ΔT) averaged in the TAUS (Figs. 5c and 6a) undergoes a positive decadal trend in austral spring (in September-October, see yellow shading in Figs. 5c and 6), followed by a strong negative trend in austral summer (in December-February, see blue shading in Figs. 5c and 6). These variations in ΔT MDT shape the significant warming trend observed in the TAUS SST in austral summer (Fig. 3b). The analysis of the contribution of each process driving the MLT changes revealed that **SFORC** warms the TAUS ML throughout the year (see Fig. 4c and Section 3.2) and this warming has steadily increased during the last three decades as shown by the positive **SFORC** linear MDT in Fig. 6a, b. The **SFORC** decadal trends are driven by both the MLD MDT and Q_{net} (see Eq. 1). Figure 6b shows that for most of the year, Q_{net} undergoes a decadal increase and, associated with a shallowing of the MLD, **SFORC** exhibits a positive MDT. In May-June and October-January, despite the decadal decrease of Q_{net} , the **SFORC** MDT remains positive, controlled by the decadal shallowing of the thin TAUS MLD. On the other hand, **V-MIX** cools the MLT all year long (Fig. 4c) and as expected, this cooling has also gradually increased in the recent decades (negative **V-MIX** MDT in Fig. 6a, b), in response to the decadal shallowing of the MLD and the positive decadal trend in **SFORC**, especially in the late austral spring and summer (October-January). The summed-up

Fig. 6 **a** and **c** are the same as in Fig. 4c, e, but for the MDT of the monthly heat budget contributions in the TAUS ($[8^{\circ}\text{S}-15^{\circ}\text{S}]$ 1° -wide coastal band). **b** shows the **SFORC** (red line), **V-MIX** (purple line), the summed-up contribution of **SFORC** and **V-MIX** (dashed orange line), **Qnet** (dashed light coral line), and **MLD MDT** (dark dashed green line), along with **DT MDT** (black line). **d** shows the **Y-ADV** MDT computed online by the model (dashed cyan line), along with the **Y-ADV** calculated offline using climatological meridional temperature gradients (dashed red line) and the **Y-ADV** calculated offline using climatological meridional currents (dashed blue line). Yellow and blue shadings highlight focus periods of warming and cooling decadal trends, respectively. Unit is $^{\circ}\text{C}/\text{month}/\text{dec}$. The figure was created using the Matlab software (<https://mathworks.com>)

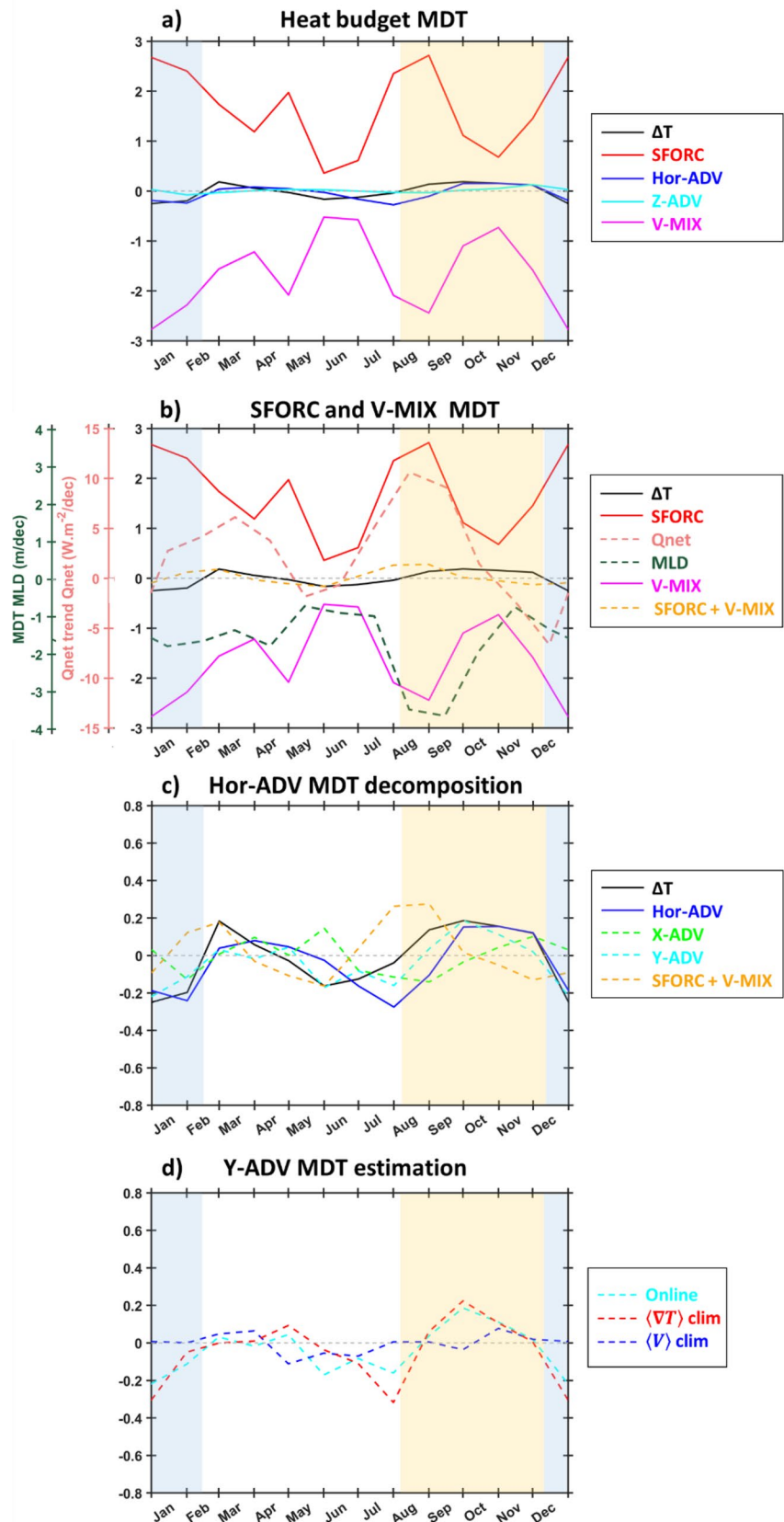
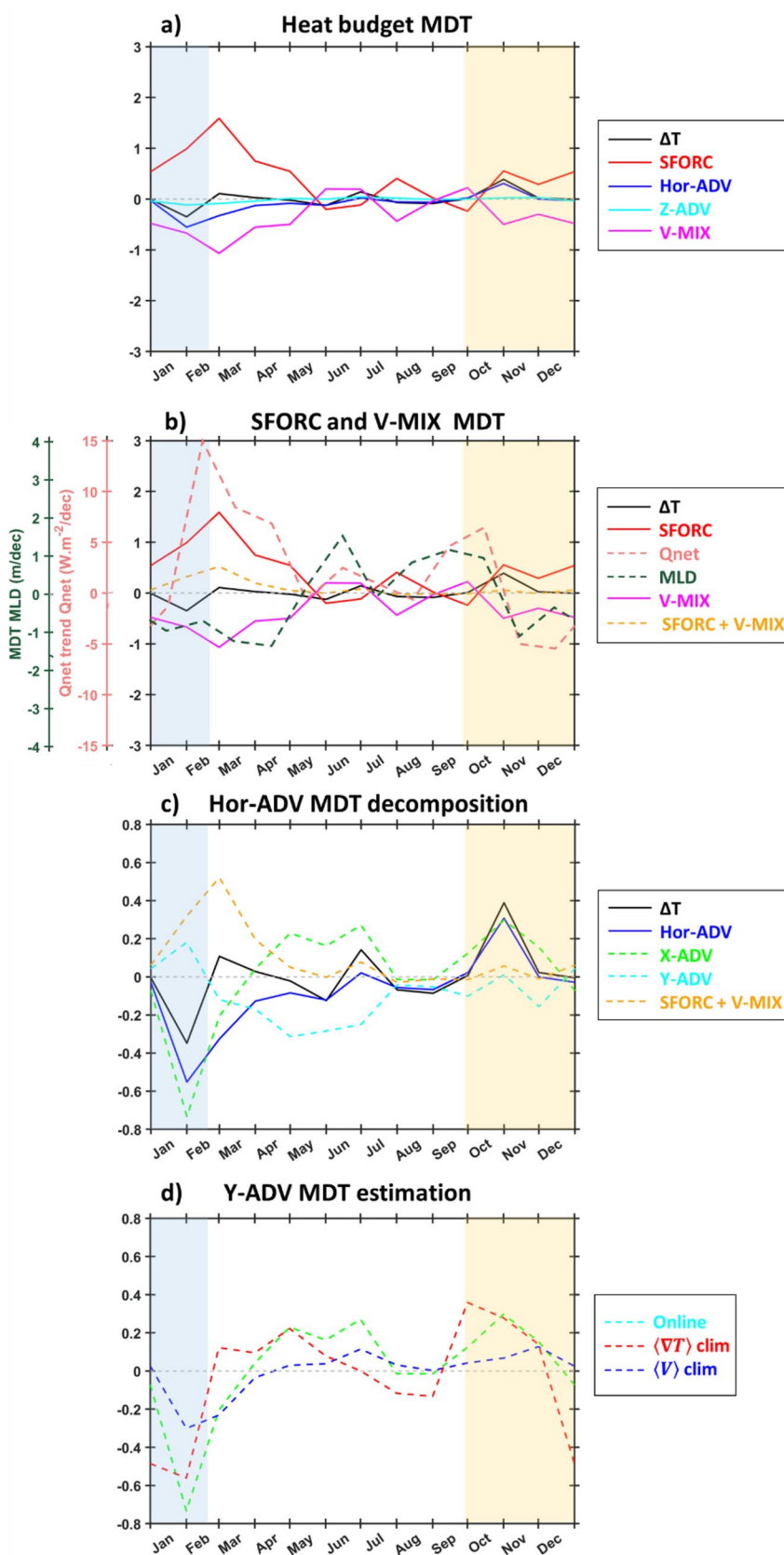


Fig. 7 Same as Fig. 6, but for the NBUS region ($[18^{\circ}\text{S}-25^{\circ}\text{S}]$ 1° -wide coastal band). The figure was generated using the Matlab software (<https://mathworks.com>)



contribution of **SFORC** and **V-MIX** MDTs is in the same order of magnitude as ΔT MDT (Fig. 6b, c) but is out of phase with it in austral spring and summer. It exhibits a warming trend in late austral summer (February–March) and late winter (July–September), while it results in a cooling trend during the rest of the year.

Focusing on the advection terms, we report that **Z-ADV** MDT remains remarkably weak (Fig. 6a), generally close to zero, except in early austral summer, when it shows a small positive trend ($\sim +0.1$ °C/month/dec). This implies a slight reduction of the austral summer cooling rate (Fig. 4c). For its part, the **Hor-ADV** warms the TAUS ML in austral spring (positive **Hor-ADV** in September–November, Fig. 4c), and this warming has increased up to $+0.15$ °C/month/dec during the last decades (Fig. 6a, c). In austral summer, autumn, and winter, the **Hor-ADV** cools the TAUS ML (Fig. 4c), and this cooling effect has increased in austral summer and winter (negative **Hor-ADV** MDT in December–February and June–September Fig. 6ac), while it has reduced in austral autumn (positive **Hor-ADV** MDT in Fig. 6a, c). Interestingly, the **Hor-ADV**, identified as the dominant process driving the climatological MLT variations in the TAUS in austral spring (see Section 3.2), exhibits a MDT (blue line in Fig. 6ac) almost identical to the ΔT MDT. This suggests that the long-term intensification of the austral spring warming can be attributed to the decadal changes of the coastal **Hor-ADV**. Similarly, the demise of the long-term summer warming is mainly due to the increase of the **Hor-ADV** cooling during this period.

Further decomposition of the **Hor-ADV** into its zonal (**X-ADV**) and meridional (**Y-ADV**) components (Fig. 6c) shows that the positive and negative trends of **Hor-ADV** during the austral spring and summer are predominantly driven by the trends in the meridional advection process (**Y-ADV**, cyan dashed line). At last, we conducted a decomposition of the monthly **Y-ADV** in the TAUS to disentangle the part of the **Y-ADV** MDT attributed to the long-term changes in the coastal currents from the part associated with the changes in the MLT horizontal gradients. Therefore, we re-evaluated the **Y-ADV** offline, assuming in the first case that the MLT gradients remain climatological, and in the second case, that it is rather the ML currents that do not vary interannually. The results, presented in Fig. 6d, reveal that the **Y-ADV** MDT with climatological meridional gradients (dashed red line) remains in very good agreement with the online estimation of the **Y-ADV** MDT (dashed cyan line), especially in the austral summer and spring. This indicates that the onset and demise of the warming trend observed off Angola in austral spring and summer (Fig. 3b, Fig. 5a, c) is associated with the modulation of the Angola Current.

In the NBUS (Fig. 7), the heat budget terms exhibit noisier MDTs compared to the trends observed in the TAUS, showing alternating positive and negative decadal

trends depending on the calendar month. The MDT of the summed-up contribution of all processes (ΔT), as described in the previous section (Fig. 5d), undergoes a positive decadal trend in late austral spring and early summer (up to $+0.4$ °C/month/dec in September–November, see yellow shading in Figs. 5d and 7), followed by strong negative trends in austral summer (< -0.3 °C/month/dec in January–February, see blue shading in Figs. 5d and 7). These variations in ΔT MDT shape the significant warming and cooling trends observed in the NBUS SST in austral summer and autumn, respectively (Fig. 3b). The analysis of the contribution of each process driving the MLT MDT shows that the seasonal warming associated with **SFORC** (Fig. 4d) has increased in late austral spring and summer during the last three decades (positive **SFORC** MDT in October–February in Fig. 7a, b), mainly associated with a decadal shallowing of the MLD in this period of the year. The seasonal cooling associated with **V-MIX** (Fig. 4d) has increased during late austral spring and summer over the last three decades (negative **V-MIX** MDT in Fig. 7a, b), counterbalancing **SFORC** MDT. The residual, resulting from the summation of the **SFORC** and **V-MIX** MDTs (Fig. 7bc), exhibits a positive trend in austral summer, while it has not significantly changed during the rest of the year.

The **Z-ADV** MDT in NBUS (Fig. 7a) also remains remarkably weak, as in the TAUS, generally hovering around zero, except in austral summer when a negative trend of up to -0.12 °C/month/dec is reported. The **Hor-ADV**, on other hand, cools the NBUS ML all year long (Fig. 4d), and this cooling effect has reduced in late austral spring (positive **Hor-ADV** MDT in October–November in Fig. 7a, c), while it has increased during the rest of the year (negative **Hor-ADV** MDT in Fig. 7a, c). Furthermore, the **Hor-ADV**, although not the dominant process driving the MLT variation, exhibits an MDT almost identical to the ΔT MDT in the late austral winter, spring, and summer. This suggests that the long-term intensification of the early austral summer warming in the NBUS can be attributed to the decrease of the **Hor-ADV** cooling during this period. Similarly, the long-term cooling in late austral summer and late winter can be attributed to the increase of the **Hor-ADV**. The analysis of the **Hor-ADV** components (Fig. 7c) further reveals that the **X-ADV** MDT is the main driver of the **Hor-ADV** MDT in the NBUS. Similar to the TAUS, the offline decomposition of the advection term presented in Fig. 7d also shows that the decadal changes in the zonal heat transport (dashed green line) are driven by the change in the amplitude of the coastal current (dashed blue line) rather than the changes in the MLT gradients.

In summary, the decadal changes in the coastal ocean circulation are the main drivers of the MLT trend in both the TAUS and the NBUS. In the following section, we

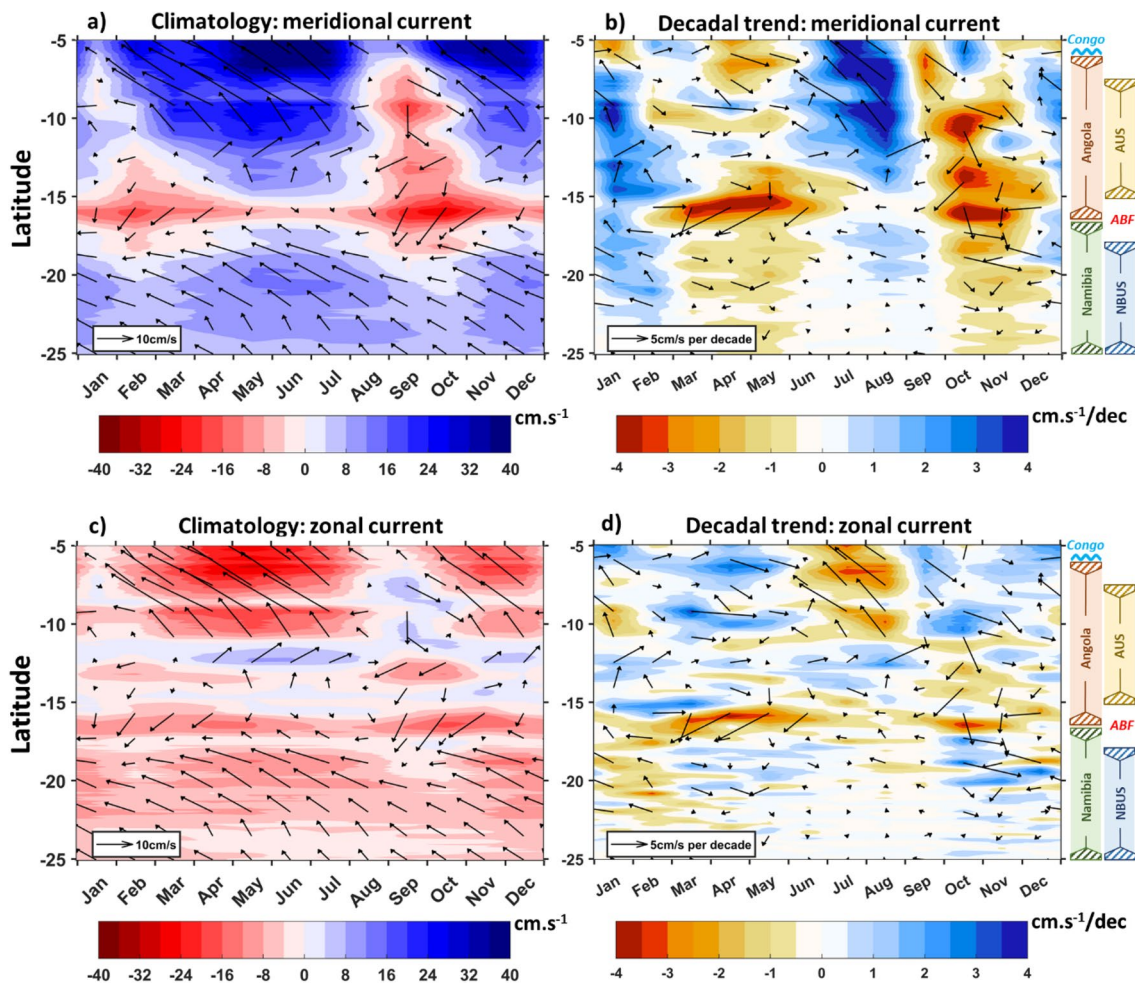


Fig. 8 Latitude-time Hovmöller diagrams of: **a** the coastal (averaged in the 1°-wide coastal band) climatological horizontal current averaged in the ML (cm.s^{-1} , arrows) and its meridional component (cm.s^{-1} , shading). **b** Same as **a** but for the MDT ($\text{cm.s}^{-1}/\text{dec}$). **c** Same as

a but for the zonal current. **d** Same as **c** but for the MDT ($\text{cm.s}^{-1}/\text{dec}$). The figure was created using the Matlab software (<https://mathworks.com>)

therefore analyze the MDT of the horizontal coastal currents along the coast of Angola and Namibia.

3.5 Role of the horizontal current evolution in the seasonal trend

The current averaged in the surface ML display a pronounced seasonal cycle (Fig. 8a, c), which is particularly strong in the coastal Angolan region. The meridional component of the coastal currents in the TAUS flows southward in January-February and August-October, and reverses to north during the rest of the year, reaching intensities of up to 18 cm.s^{-1} in agreement with Awo et al. (2022). The southward flow is strong in August-October with maximum values up to 16 cm.s^{-1} in September, while it is weaker in January-February with values less than 6 cm.s^{-1} . In agreement with Awo et al. (2022), the southward current extends vertically

below the ML (not shown), while the northward current is observed only within the ML. In the ABF region, the meridional current flows consistently southward throughout the year, with two maxima. The first peak, with intensities up to 14 cm.s^{-1} , is observed in February, while the second maximum, with values up to 28 cm.s^{-1} , is prominent in September-October. Further south, in the NBUS region, the current maintains a northwestward flow throughout the year, with maximum values up to 14 cm.s^{-1} in austral winter. The MDT analysis of the horizontal ML currents (Fig. 8b) shows that the southward current in the TAUS has intensified up to $3 \text{ cm.s}^{-1}/\text{dec}$ in September-October over the last three decades. Conversely, the northward current has weakened by $2.5 \text{ cm.s}^{-1}/\text{dec}$ in November, both contributing to the TAUS warming trend in austral spring. Similarly, in the austral summer, the northward current has strengthened by up to $4 \text{ cm.s}^{-1}/\text{dec}$ in December-January and the southward current

has weakened up to $-3 \text{ cm.s}^{-1}/\text{dec}$ in February, explaining the negative trend depicted in **Y-ADV**. During the austral winter, the TAUS northward current has increased by up to $4 \text{ cm.s}^{-1}/\text{dec}$. In summary, the fluctuations of the MDT of the Angola Current are in agreement with the TAUS **Y-ADV** MDTs described previously (Fig. 6c).

In the NBUS, the trend analysis shows weak trends in the equatorward current. The Benguela Current has weakened by up to $1.5 \text{ cm.s}^{-1}/\text{dec}$ in austral autumn and late spring, while the trend remains almost negligible in austral winter and early spring. Focusing on the zonal component of the current, the results show that the westward current has weakened up to $1.5 \text{ cm.s}^{-1}/\text{dec}$ in October–December contributing to reduce the offshore transport of upwelled coastal water. Conversely, the westward current has intensified by $2 \text{ cm.s}^{-1}/\text{dec}$ in January–February, contributing to enhance the coastal divergence. This increase in the westward current is also observed in August–September but it remains very weak and not significant. In summary, the MDT variations in the zonal component of the Benguela Current explains the **X-ADV** MDT in NBUS (Fig. 7c).

4 Discussion and conclusions

In this study, we analyzed the climatology of the long-term changes of the upper layer temperature in the productive marine ecosystems of the southeastern tropical Atlantic off Angola (TAUS) and Namibia (NBUS). We investigated the main processes responsible for these changes based on the analysis of the ML heat budget from a $\sim 9 \text{ km}$ resolution regional ocean model over the period 1982–2015.

Our results revealed a clear seasonal dependence of the decadal SST trends in the first 100 km (1° band along the coast) along the Angolan and Namibian coasts. The overall annual warming trend in the TAUS is mainly the result of a pronounced warming trend in late austral spring and summer (October–January), with no significant change observed in austral autumn and winter (February–September). In contrast to the TAUS, the weak annual trend in the NBUS results from a counterbalance of the austral winter cooling trend and the austral summer warming trend.

To better understand the mechanisms underlying these long-term changes, we first provided an overview of the mean processes driving the model climatological surface temperature variations in both the TAUS and the NBUS. At the climatological scale, the coastal ML of the TAUS and NBUS cools during the austral autumn/winter and warms throughout the rest of the year. Heat budget analysis showed that the surface forcing (**SFORC**) warms the coastal ML throughout the year along the entire southwest African coast, while the vertical mixing (**V-MIX**) distributes this heat below the ML, counterbalancing the atmospheric surface

warming. Their combined contribution results in a warming of the ML, especially during the austral summer. In austral winter, both horizontal and vertical advections (**Hor-ADV** and **Z-ADV**) contribute to the cooling of the ML in both regions. Conversely, in austral summer, it is the combined contribution of the atmospheric surface forcing and the **Hor-ADV** that warms the coastal ML. Notably, in austral spring in the TAUS, we show that the **Hor-ADV** emerges as the main contributor to the ML warming, in agreement with Awo et al. (2022), highlighting the importance of the mean horizontal advection during this season.

On the analysis of the processes driving the long-term surface temperature changes, our results showed that, whilst the TAUS and the NBUS undergo different dynamics, their climatological long-term trends are driven by the same process, i.e. the **Hor-ADV**. The **Hor-ADV** controls the monthly climatological decadal warming trend of the austral spring and summer ML in the TAUS. It also controls the austral summer ML warming trend and the late austral winter and spring cooling trends in the NBUS. In both regions, the contribution of the decadal changes in **Z-ADV** and the sum of **SFORC** and **V-MIX** terms remains small during these periods. These results differ from those reported by Vizy et al. (2018), which may be due to a divergence in modeling strategy. In fact, they used a regional climate model run at a coarse resolution, composed of the Weather Research and Forecasting Model (Skamarock et al. 2008) coupled to a one-layer ocean model which may misrepresent the coastal currents. Note that the resolution of our model surface forcing is also relatively coarse ($0.7^\circ \times 0.7^\circ$) compared to the resolution of our CROCO configuration ($1/12^\circ$, see Section 2.2). In particular, the coastal cloud cover and the decrease in the wind amplitude as one approaches the coast may not be well represented in the DFS forcing, resulting in a warm bias in the mean SST off Namibia (see supplementary material in Illig et al. 2020). A sensitivity test could be performed by using outputs from the matching WRF regional atmospheric model configuration at $0.25^\circ \times 0.25^\circ$ developed in Illig and Bachèlery (2024).

Our study confirmed the critical contribution of **SFORC** and **V-MIX** to the seasonal variations of the surface ML in both coastal systems, consistent with previous studies (Scanell and McPhaden 2018; Körner et al. 2023). However, a series of sensitivity tests (not shown) highlighted the excessive dependence of the magnitude of **SFORC** and **V-MIX** on the choice of the surface layer thickness. A deeper surface ML reduces the contribution of **SFORC** and **V-MIX** terms, even leading to their reversal, while the magnitude of the advection terms remains relatively stable, with no significant changes in their contribution. These results improve our understanding of the intricate interplay between **SFORC** and **V-MIX** processes, and the MLD. On monthly climatological decadal scales, the variations in MLD also drive the trends in **SFORC**

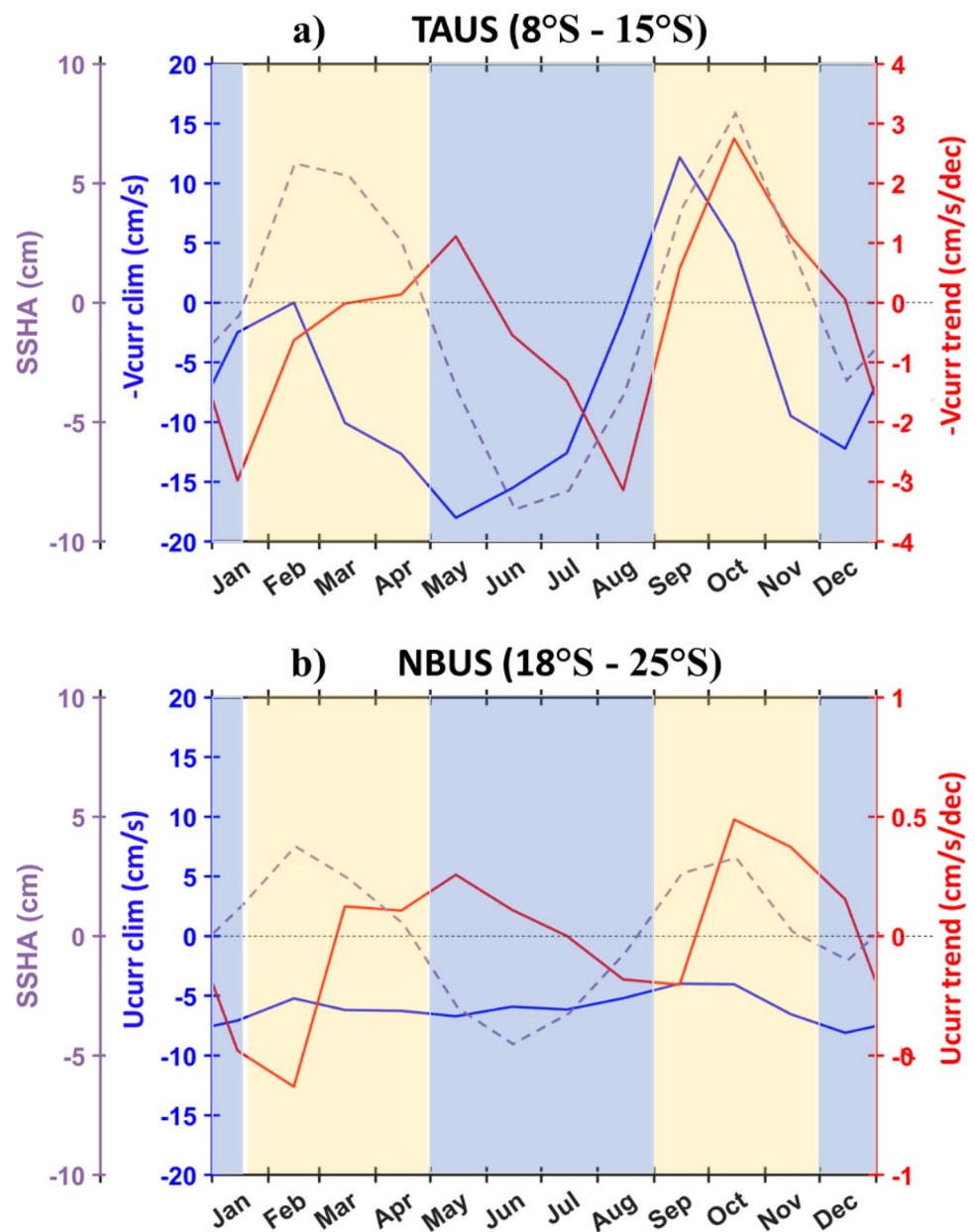
and **V-MIX**. Our modeling results show a shallowing trend of the MLD in the TAUS, in contrast to the study by Vizzy et al. (2018), where the prescribed MLD deepens. Nevertheless, the **Hor-ADV** is the main process at work to explain the climatological decadal trend of the SST off southwest Africa, so our results do not ultimately depend on the chosen MLD or its decadal variations.

We further disentangled the role of currents vs. horizontal gradients in the contribution of zonal and meridional advections. Our analyses showed that, in both regions, the changes in the **Hor-ADV** are primarily attributed to changes in the coastal currents. In the TAUS, the warming trend of the MLT in austral spring and early summer, followed by its demise in late austral summer, can be attributed to the

southward intensification of the Angola Current. This current brings warm water from the equator into the region in austral spring and early summer, while the northward intensification of the reverse Angola Current in late austral summer contributes to the dissipation of this warming trend. Similarly, in the NBUS, the warming trend of the MLT during the austral early summer can be attributed to a weakening of the northwestward Benguela Current, which brings cold water from the south into the NBUS region.

Interestingly, the decadal changes in the coastal current can be related to a long-term modulation of the seasonal equatorially-forced CTWs, because (1) the decadal changes in the meridional current show a coherent pattern from the equator to the NBUS (Fig. 8b), and (2) because there is

Fig. 9 Comparison of climatology of the current (blue line, cm/s) and its trend (red line, cm/s/dec) and the CTWs using SSH anomaly as proxy for CTWs (purple dashed line cm) in (a) the TAUS ([8°S–15°S] 1°-wide coastal band) for meridional current, and (b) the NBUS ([18°S–25°S] 1°-wide coastal band) for zonal current same as panel (a). Yellow and blue highlight the Downwelling and the upwelling CTWs respectively for the TAUS region. The figure was created using the Matlab software (<https://mathworks.com>)



a seasonal phase between the climatological trend of the coastal currents and the passage of the seasonal equatorially-forced CTWs off Angola (Fig. 9a). In spring the southward intensification of the Angola Current coincides with the passage of the seasonal downwelling CTW. Similarly, in the NBUS, the weakening of the northwestward Benguela Current in austral spring coincides with the passage of the downwelling CTWs (Fig. 9b). Notably, the downwelling CTWs and the associated change in the current are in phase with the MLT warming trend in the TAUS but are shifted by one month in the NBUS. This temporal shift could be attributed to the pronounced cooling trend of the MLT in the preceding spring, which conceals the onset of the warming trend associated with the weakening of the Benguela Current and the passage of the downwelling CTWs (Fig. 9b). It's worth noting that Bachèlery et al. (2020) and (Körner et al. 2024) also emphasized this connection with the equatorial variability, suggesting that changes in the magnitude of equatorially-forced CTW activity could lead to decadal modulation of the Angolan and Namibian coastal variability. This insight implies decadal changes in the equatorial winds triggering the equatorial forcing.

In the TAUS, the warming trend in the austral summer results in an increase in the amplitude of the seasonal cycle of the MLT (Fig. 10), which may affect the ecosystem and the climate in the tropical Atlantic. For instance, Awo et al. (2022) showed that low salinity water is advected into the TAUS in spring by the poleward Angola current. In our study, we show that this poleward current has significantly intensified over the last three decades, potentially leading to increased advection of low salinity water into the region on a long-term scale. In addition, the increased advection of warm water southward may enhance the upper ocean stratification which would reduce the early austral summer minor upwelling of cool subsurface water into the ML. However, in austral winter, no significant changes are observed (Figs. 3b, c and 10).

From an ecological perspective, the presented decadal trend distributions provide an indication of which coastal regions within the studied domain are climatologically more favourable for fish reproduction than others. Fish exhibit the narrowest thermal tolerance range during the reproduction phase compared to the other life cycle stages. Reproductive performance, and thus future population size, is most vulnerable to even slight deviations from the optimal thermal range induced by ocean warming (Dahlke et al. 2020). In the case of *Sardinella aurita*, the dominant small pelagic fish in the TAUS, the optimal reproductive temperature range is in the low twenties Celsius (Ettahiri et al. 2003), which falls during the austral winter (Fig. 10). According to (Fig. 3b, c), the region north of about 13°S has not experienced decadal warming during winters. Since the reproductive habitat of *Sardinella aurita* is restricted to the same area (Boely and

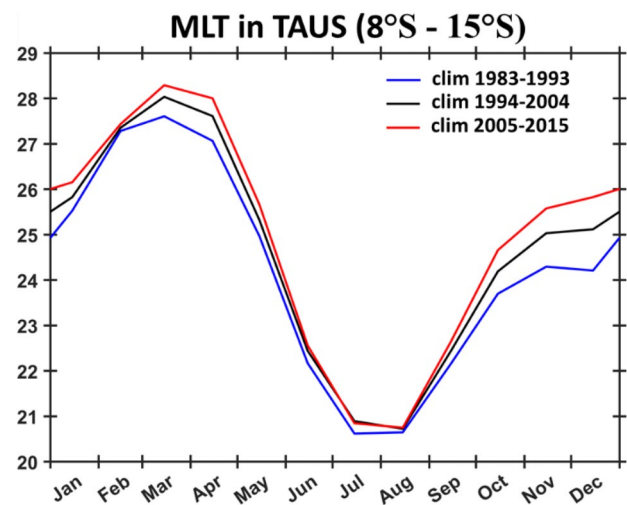


Fig. 10 Seasonal cycle of MLT in the TAUS over different periods: 1983–1993 (blue), 1994–2004 (black), and 2005–2015 (red). The figure was created using the Matlab software (<https://mathworks.com>)

Fréon 1980; Ghéno and Fontana 1981), the above observation leads to the conjecture that the reproduction of the Angolan *Sardinella* has probably not been affected by the ocean warming during the decades of this analysis. This conclusion is corroborated by the results of stock assessment surveys covering approximately during the same time period, which show interannual fluctuations but the stable size of the Angolan *Sardinella* population on the decadal timescale (FAO 2011), consistent with the prediction inferred from the presented MDT. Conversely, (Fig. 3b, c) indicates a MDT during winter in the southern Angola region, 13°–17°S, suggesting a detrimental impact on the coastal fish populations resident there. A study by (Potts et al. 2014) examined the effect of ocean warming in this region on the distribution of coastal resident fish species and concluded, in line with the above expectation, that decadal SST trends have resulted in significant poleward shifts of the areas favorable for their reproduction and to a decrease in the population size.

Acronyms

°C/dec: Degree Celsius per decade; **ABF:** Angola Benguela Front; **CTWs:** Coastal Trapped Waves; **DFS:** DRAKKAR Forcing Set (version 5.2); **MDT:** Monthly climatological Decadal Trend; **LDT:** Long-term Decadal Trend; **ML:** Mixed Layer; **MLT:** Mixed Layer Temperature; **MLD:** Mixed Layer Depth; **NBUS:** North Benguela Upwelling System (18°S–25°S); **Qnet:** Net surface heat flux; **SST:** Sea Surface Temperature; **TAUS:** Tropical Angola Upwelling System (8°S–15°S)

Heat budget analysis

ΔT: Rate of change of the mixed-layer temperature;
X-ADV: Zonal Advection; **Y-ADV:** Meridional Advection;

Hor-ADV: Horizontal Advection; **Z-ADV:** Vertical Advection; **V-MIX:** Vertical Mixing; **SFORC:** Surface atmospheric heat Forcing

Supplementary Information The online version contains supplementary material available at <https://doi.org/10.1007/s00382-024-07305-z>.

Acknowledgements We would like to extend our heartfelt thanks to Isabelle Ansorge, Jennifer Veitch and the Department of Oceanography at the University of Cape Town for their unwavering support during the difficult time following Mathieu's death. This work is part of the TRIATLAS European project (South and Tropical Atlantic climate-based marine ecosystem prediction for sustainable management; H2020 Grant agreement No 817578). Folly Serge Tomety and Founi Mesmin Awo post-doctoral fellowships was also funded by Nansen Tutu Center for Marine Environmental Research, Department of Oceanography, University of Cape Town, Cape Town, South Africa and the NRF Sarchi Chair on Ocean Atmosphere Modeling, the Belmont Forum CRA Transdisciplinary Research for Ocean Sustainability (Ocean 2018). This work is a contribution to EXEBUS (Ecological and Economic impacts of the intensification of extreme events in the Benguela Upwelling System) project (309347) funded by the Research Council of Norway PCO2. Marie-Lou Bachèlery has received funding from the European Union's Horizon 2020 Research and Innovation Program for the project BENGUP under the Marie Skłodowska-Curie grant agreement ID 101025655. Model computations were performed on CALMIP computer at University Paul Sabatier (Toulouse, France, CALMIP, project 19002).

Author contributions Folly Serge Tomety, Mathieu Rouault, and Noel Keenlyside conceived and designed the study. Material preparation and analyses were performed by Folly Serge Tomety and Serena Illig. Folly Serge Tomety and Serena Illig co-wrote the original draft. Review and editing were performed by Founi Mesmin Awo, Marie-Lou Bachèlery, Marek Ostrowski, and Noel Keenlyside.

Funding Open access funding provided by University of Cape Town. Folly Serge Tomety and Founi Mesmin Awo have received funding from TRIATLAS and EXEBUS. Marie-Lou Bachèlery was supported funding from BENGUP.

Data availability The datasets generated and analyzed during the current study, due to their large size, are not publicly available, but are available from the corresponding author on reasonable request.

Declarations

Financial interests The authors have no financial interests to disclose.

Competing interests The authors have not disclosed any competing interests.

Open Access This article is licensed under a Creative Commons Attribution 4.0 International License, which permits use, sharing, adaptation, distribution and reproduction in any medium or format, as long as you give appropriate credit to the original author(s) and the source, provide a link to the Creative Commons licence, and indicate if changes were made. The images or other third party material in this article are included in the article's Creative Commons licence, unless indicated otherwise in a credit line to the material. If material is not included in the article's Creative Commons licence and your intended use is not permitted by statutory regulation or exceeds the permitted use, you will

need to obtain permission directly from the copyright holder. To view a copy of this licence, visit <http://creativecommons.org/licenses/by/4.0/>.

References

- Alory G, Meyers G (2009) Warming of the upper equatorial Indian Ocean and changes in the heat budget (1960–99). *J Clim* 22(1):93–113. <https://doi.org/10.1175/2008JCLI2330.1>
- Awo FM, Rouault M, Ostrowski M, Tomety F, Da-Allada C, Jouanno J (2022) Seasonal cycle of sea surface salinity in the Angola Upwelling System. *J Geophys Res: Oceans* 127(7):e2022JC018518. <https://doi.org/10.1029/2022JC018518>
- Bachèlery ML, Illig S, Dadou I (2016) Interannual variability in the South-East Atlantic Ocean, focusing on the Benguela Upwelling System: remote versus local forcing. *J Geophys Res: Oceans* 121(1):284–310. <https://doi.org/10.1002/2015JC011168>
- Bachèlery M-L, Illig S, Rouault M (2020) Interannual coastal trapped waves in the Angola-Benguela upwelling system and Benguela Niño and Niña events. *J Mar Syst* 203:103262. <https://doi.org/10.1016/j.jmarsys.2019.103262>
- Binet D, Gobert B, Maloueki L (2001) El Nino-like warm events in the Eastern Atlantic (6 N, 20 S) and fish availability from Congo to Angola (1964–1999). *Aquat Living Resour* 14(2):99–113. [https://doi.org/10.1016/S0990-7440\(01\)01105-6](https://doi.org/10.1016/S0990-7440(01)01105-6)
- Blamey LK, Shannon LJ, Bolton JJ, Crawford RJ, Dufois F, Evers-King H, Griffiths CL, Hutchings L, Jarre A, Rouault M (2015) Ecosystem change in the southern Benguela and the underlying processes. *J Mar Syst* 144:9–29. <https://doi.org/10.1016/j.jmarsys.2014.11.006>
- Boely T, Fréon P (1980) Coastal pelagic resources. In: *The Fish Resources of the Eastern Central Atlantic. Part One: The Resources of the Gulf of Guinea from Angola to Mauritania*, in FAO Fisheries Technical Paper No. 186.1, edited by J. P. Troade and S. Garcia, pp 13–76
- Bordbar MH, Mohrholz V, Schmidt M (2021) The relation of wind-driven coastal and offshore upwelling in the Benguela upwelling system. *J Phys Oceanogr* 51(10):3117–3133. <https://doi.org/10.1175/jpo-d-20-0297.1>
- Boyer D, Boyer H, Fossen I, Kreiner A (2001) Changes in abundance of the northern Benguela sardine stock during the decade 1990–2000, with comments on the relative importance of fishing and the environment. *Afr J Mar Sci* 23:67–84. <https://doi.org/10.2989/025776101784528854>
- Brandt P, Bordbar MH, Coelho P, Koungue RAI, Körner M, Lamont T, Lübbecke JF, Mohrholz V, Prigent A, Roch M (2024) Physical drivers of Southwest African coastal upwelling and its response to climate variability and change, in *Sustainability of Southern African Ecosystems under Global Change: Science for Management and Policy Interventions*, edited, pp 221–257, Springer. https://doi.org/10.1007/978-3-031-10948-5_9
- Carr M, Lamont T, Krug M (2021) Satellite sea surface temperature product comparison for the southern African marine region. *Remote Sens* 13(7):1244. <https://doi.org/10.3390/rs13071244>
- Chen Z, Yan X-H, Jo Y-H, Jiang L, Jiang Y (2012) A study of Benguela upwelling system using different upwelling indices derived from remotely sensed data. *Cont Shelf Res* 45:27–33. <https://doi.org/10.1016/j.csr.2012.05.013>
- Cury P, Roy C (1989) Optimal environmental window and pelagic fish recruitment success in upwelling areas. *Can J Fish Aquat Sci* 46(4):670–680. <https://doi.org/10.1139/f89-086>
- Dahlke FT, Wohlrab S, Butzin M, Pörtner H-O (2020) Thermal bottlenecks in the life cycle define climate vulnerability of fish.

- Science 369(6499):65–70. <https://doi.org/10.1594/PANGAEA.917796>
- Debreu L, Marchesiello P, Penven P, Cambon G (2012) Two-way nesting in split-explicit ocean models: algorithms, implementation and validation. *Ocean Model* 49:1–21. <https://doi.org/10.1016/j.ocemod.2012.03.003>
- Deppenmeier A-L, Haarsma RJ, van Heerwaarden C, Hazeleger W (2020) The Southeastern Tropical Atlantic SST Bias Investigated with a coupled atmosphere–ocean single-column model at a PIRATA Mooring Site. *J Clim* 33(14):6255–6271. <https://doi.org/10.1175/JCLI-D-19-0608.1>
- Dunn J (2009) CARS 2009: CSIRO atlas of regional seas. Mar lab Sci And Ind Res: Organ Hobart Rep, Tasmania. <http://www.marine.csiro.au/~dunn/cars2009/>. Accessed 16 June 2024
- Dussin R, Barnier B, Brodeau L, Molines JM (2016) The making of DRAKKAR forcing set DFS5, DRAKKAR/MyOcean, edited, Report
- Ettahiri O, Berraho A, Vidy G, Ramdani M (2003) Observation on the spawning of *Sardina* and *Sardinella* off the south Moroccan Atlantic coast (21–26 N). *Fish Res* 60(2–3):207–222. [https://doi.org/10.1016/S0165-7836\(02\)00172-8](https://doi.org/10.1016/S0165-7836(02)00172-8)
- FAO (2011) Review of the State of World Marine Fishery Resources. In: Resources Fisheries Technical Paper, edited, FAO, Rome, p 335
- Florenchie P, Lutjeharms JR, Reason C, Masson S, Rouault M (2003) The source of Benguela Niños in the south Atlantic Ocean. *Geophys Res Lett* 30(10). <https://doi.org/10.1029/2003GL017172>
- García-Reyes M, Sydeman WJ, Schoeman DS, Rykaczewski RR, Black BA, Smit AJ, Bograd SJ (2015) Under pressure: climate change, upwelling, and eastern boundary upwelling ecosystems. *Front Mar Sci* 2:109. <https://doi.org/10.3389/fmars.2015.00109>
- Ghéno Y, Fontana A (1981) Les stocks de petits pélagiques côtiers les sardinelles, Milieu marin et ressources halieutiques de la république populaire du Congo, 213–257. https://horizon.documentation.ird.fr/exl-doc/pleins_textes/pleins_textes_5/pt5/travaux_d/01222.pdf, <https://search.worldcat.org/title/808019276>
- Hjort J (1914) Fluctuations in the great fisheries of northern Europe viewed in the light of biological research. ICES
- Hourdin F, Găinuşă-Bogdan A, Braconnot P, Dufresne JL, Traore AK, Rio C (2015) Air moisture control on ocean surface temperature, hidden key to the warm bias enigma. *Geophys Res Lett* 42(24):10,885–810,893. <https://doi.org/10.1002/2015GL066764>
- Huang B, Hu Z-Z, Jha B (2007) Evolution of model systematic errors in the tropical Atlantic basin from coupled climate hindcasts. *Clim Dyn* 28:661–682. <https://doi.org/10.1007/s00382-006-0223-8>
- Huang B, Liu C, Banzon V, Freeman E, Graham G, Hankins B, Smith T, Zhang H-M (2021) Improvements of the daily optimum interpolation sea surface temperature (DOISST) version 2.1. *J Clim* 34(8):2923–2939. <https://doi.org/10.1175/JCLI-D-20-0166.1>
- Hutchings L, Van der Linden C, Shannon L, Crawford R, Verheye H, Bartholomae C, Van der Plas A, Louw D, Kreiner A, Ostrowski M (2009) The Benguela Current: an ecosystem of four components. *Prog Oceanogr* 83(1–4):15–32. <https://doi.org/10.1016/j.pocean.2009.07.046>
- Illig S, Bachelery M-L (2024) The 2021 Atlantic Niño and Benguela Niño events: external forcings and air–sea interactions. *Clim Dyn* 62(1):679–702
- Illig S, Dewitte B, Goubanova K, Cambon G, Boucharel J, Monetti F, Romero C, Purca S, Flores R (2014) Forcing mechanisms of intraseasonal SST variability off central Peru in 2000–2008. *J Geophys Res: Oceans* 119(6):3548–3573. <https://doi.org/10.1002/2013JC009779>
- Illig S, Bachelery ML, Lübbecke JF (2020) Why do benguela Niños lead atlantic Niños? *J Geophys Res: Oceans* 125(9):e2019JC016003. <https://doi.org/10.1029/2019JC016003>
- Junker T, Schmidt M, Mohrholz V (2015) The relation of wind stress curl and meridional transport in the Benguela upwelling system. *J Mar Syst* 143:1–6. <https://doi.org/10.1016/j.jmarsys.2014.10.006>
- Kendall MG (1948) Rank correlation methods. <https://doi.org/10.1017/S0020268100013019>
- Kondo J (1975) Air-sea bulk transfer coefficients in diabatic conditions. *Boundary Layer Meteorol* 9:91–112. <https://doi.org/10.1007/BF00232256>
- Kopte R, Brandt P, Dengler M, Tchipalanga P, Macuéria M, Ostrowski M (2017) The Angola Current: Flow and hydrographic characteristics as observed at 11 S. *J Geophys Research: Oceans* 122(2):1177–1189. <https://doi.org/10.1002/2016JC012374>
- Körner M, Brandt P, Dengler M (2023) Seasonal cycle of sea surface temperature in the tropical Angolan Upwelling System. *Ocean Sci* 19(1):121–139. <https://doi.org/10.5194/os-19-121-2023>
- Körner M, Brandt P, Illig S, Dengler M, Subramaniam A, Bachelery M-L, Krahmann G (2024) Coastal trapped waves and tidal mixing control primary production in the tropical Angolan upwelling system. *Sci Adv* 10(4):eadj6686. <https://doi.org/10.1126/sciadv.adj6686>
- Koseki S, Keenlyside N, Demissie T, Toniazzo T, Counillon F, Bethke I, Ilıcak M, Shen M-L (2018) Causes of the large warm bias in the Angola–Benguela Frontal Zone in the Norwegian Earth System Model. *Clim Dyn* 50(11–12):4651–4670. <https://doi.org/10.1007/s00382-017-3896-2>
- Kurian J, Li P, Chang P, Patricola CM, Small J (2021) Impact of the Benguela coastal low-level jet on the southeast tropical Atlantic SST bias in a regional ocean model. *Clim Dyn* 56:2773–2800. <https://doi.org/10.1007/s00382-020-05616-5>
- Large WG, McWilliams JC, Doney SC (1994) Oceanic vertical mixing: a review and a model with a nonlocal boundary layer parameterization. *Rev Geophys* 32(4):363–403. <https://doi.org/10.1029/94RG01872>
- Lutz K, Jacobeit J, Rathmann J (2015) Atlantic warm and cold water events and impact on African west coast precipitation. *Int J Climatol* 35(1):128–141. <https://doi.org/10.1002/joc.3969>
- Mann HB (1945) Nonparametric tests against trend. *Econometrica: J Econ Soc* 245–259. <https://doi.org/10.2307/1907187>
- Marchesiello P, McWilliams JC, Schepetkin A (2001) Open boundary conditions for long-term integration of regional oceanic models. *Ocean Model* 3(1–2):1–20. [https://doi.org/10.1016/S1463-5003\(00\)00013-5](https://doi.org/10.1016/S1463-5003(00)00013-5)
- Mohrholz V, Bartholomae C, Van der Plas A, Lass H (2008) The seasonal variability of the northern Benguela undercurrent and its relation to the oxygen budget on the shelf. *Cont Shelf Res* 28(3):424–441. <https://doi.org/10.1016/j.csr.2007.10.001>
- Ostrowski M, Da Silva JC, Bazik-Sangolay B (2009) The response of sound scatterers to El Niño-and La Niña-like oceanographic regimes in the southeastern Atlantic. *ICES J Mar Sci* 66(6):1063–1072. <https://doi.org/10.1093/icesjms/fsp102>
- Penven P, Debreu L, Marchesiello P, McWilliams JC (2006) Evaluation and application of the ROMS 1-way embedding procedure to the central California upwelling system. *Ocean Model* 12(1–2):157–187. <https://doi.org/10.1016/j.ocemod.2005.05.002>
- Polo I, Lazar A, Rodriguez-Fonseca B, Arnault S (2008) Oceanic Kelvin waves and tropical Atlantic intraseasonal variability: 1. Kelvin wave characterization. *J Geophys Res: Oceans* 113(C7). <https://doi.org/10.1029/2007JC004495>
- Potts WM, Booth AJ, Richardson TJ, Sauer WH (2014) Ocean warming affects the distribution and abundance of resident fishes by changing their reproductive scope. *Rev Fish Biol Fish* 24:493–504. <https://doi.org/10.1007/s11660-013-9329-3>
- Rayner N, Parker DE, Horton E, Folland C, Alexander L, Rowell D, Kent E, Kaplan A (2003) Global analyses of sea surface temperature, sea ice, and night marine air temperature since the late

- nineteenth century. *J Geophys Res: Atmos* 108(D14):4407. <https://doi.org/10.1029/2002JD002670>
- Reynolds RW, Rayner NA, Smith TM, Stokes DC, Wang W (2002) An improved in situ and satellite SST analysis for climate. *J Clim* 15(13):1609–1625. [https://doi.org/10.1175/1520-0442\(2002\)015%3C1609:AIISAS%3E2.0.CO;2](https://doi.org/10.1175/1520-0442(2002)015%3C1609:AIISAS%3E2.0.CO;2)
- Richter I, Tokinaga H (2020) An overview of the performance of CMIP6 models in the tropical Atlantic: mean state, variability, and remote impacts. *Clim Dyn* 55(9–10):2579–2601. <https://doi.org/10.1007/s00382-020-05409-w>
- Ridgway K, Dunn J, Wilkin J (2002), Ocean interpolation by four-dimensional weighted least squares—application to the waters around Australasia. *Journal of atmospheric and oceanic technology* 19(9):1357–1375. [https://doi.org/10.1175/1520-0426\(2002\)019%3C1357:OIBFDW%3E2.0.CO;2](https://doi.org/10.1175/1520-0426(2002)019%3C1357:OIBFDW%3E2.0.CO;2)
- Rouault M (2012) Bi-annual intrusion of tropical water in the northern Benguela upwelling. *Geophys Res Lett* 39(12). <https://doi.org/10.1029/2012GL052099>
- Rouault M, Florenchie P, Fauchereau N, Reason CJ (2003) South East tropical Atlantic warm events and southern African rainfall. *Geophys Res Lett* 30(5). <https://doi.org/10.1029/2002GL014840>
- Rouault M, Illig S, Lübbecke J, Koungue RAI (2018) Origin, development and demise of the 2010–2011 Benguela Niño. *J Mar Syst* 188:39–48. <https://doi.org/10.1016/j.jmarsys.2017.07.007>
- Sabatés A, Martín P, Lloret J, Raya V (2006) Sea warming and fish distribution: the case of the small pelagic fish, *Sardinella aurita*, in the western Mediterranean. *Glob Change Biol* 12(11):2209–2219. <https://doi.org/10.1111/j.1365-2486.2006.01246.x>
- Scannell HA, McPhaden MJ (2018) Seasonal mixed layer temperature balance in the southeastern tropical Atlantic. *J Geophys Res: Oceans* 123(8):5557–5570. <https://doi.org/10.1029/2018JC014099>
- Shannon LV (1985) The Benguela ecosystem. I: evolution of the Benguela physical features and processes. *Oceanogr Mar Biol* 23:105–182
- Shchepetkin AF, McWilliams JC (2005) The regional oceanic modeling system (ROMS): a split-explicit, free-surface, topography-following-coordinate oceanic model. *Ocean Model* 9(4):347–404. <https://doi.org/10.1016/j.ocemod.2004.08.002>
- Skamarock WC, Klemp JB, Dudhia J, Gill DO, Barker D, Duda MG, Huang X-Y, Wang W, Powers JG (2008) A description of the advanced research WRF version 3 (No. NCAR/TN-475 + STR), University Corporation for Atmospheric Research, National Center for Atmospheric Research Boulder, Colorado. <https://doi.org/10.5065/D68S4MVH>, <https://doi.org/10.5065/D68S4MVH>
- Sowman M, Cardoso P (2010) Small-scale fisheries and food security strategies in countries in the Benguela current large Marine Ecosystem (BCLME) region: Angola, Namibia and South Africa. *Mar Policy* 34(6):1163–1170. <https://doi.org/10.1016/j.marpol.2010.03.016>
- Tchpalanga P, Dengler M, Brandt P, Kopte R, Macuéria M, Coelho P, Ostrowski M, Keenlyside NS (2018) Eastern boundary circulation and hydrography off Angola: building Angolan oceanographic capacities. *Bull Am Meteorol Soc* 99(8):1589–1605. <https://doi.org/10.1175/BAMS-D-17-0197.1>
- Veitch J, Florenchie P, Shillington F (2006) Seasonal and interannual fluctuations of the Angola–Benguela Frontal Zone (ABFZ) using 4.5 km resolution satellite imagery from 1982 to 1999. *Int J Remote Sens* 27(05):987–998. <https://doi.org/10.1080/0143160500127914>
- Veitch J, Penven P, Shillington F (2010) Modeling Equilibrium dynamics of the Benguela Current System. *J Phys Oceanogr* 40(9):1942–1964. <https://doi.org/10.1175/2010jpo4382.1>
- Vizy EK, Cook KH (2016) Understanding long-term (1982–2013) multi-decadal change in the equatorial and subtropical South Atlantic climate. *Clim Dyn* 46(7–8):2087–2113. <https://doi.org/10.1007/s00382-015-2691-1>
- Vizy EK, Cook KH, Sun X (2018) Decadal change of the south Atlantic ocean Angola–Benguela frontal zone since 1980. *Clim Dyn* 51:3251–3273. <https://doi.org/10.1007/s00382-018-4077-7>
- Voldoire A, Exarchou E, Sanchez-Gomez E, Demissie T, Deppenmeier A-L, Frauen C, Goubanova K, Hazeleger W, Keenlyside N, Koseki S (2019) Role of wind stress in driving SST biases in the Tropical Atlantic. *Clim Dyn* 53:3481–3504. <https://doi.org/10.1007/s00382-019-04717-0>
- Zeng Z, Brandt P, Lamb K, Greatbatch RJ, Dengler M, Claus M, Chen X (2021) Three-dimensional numerical simulations of internal tides in the Angolan upwelling region. *J Geophys Res: Oceans* 126(2):e2020JC016460. <https://doi.org/10.1029/2020JC016460>

Publisher's Note Springer Nature remains neutral with regard to jurisdictional claims in published maps and institutional affiliations.

Supporting Information for

“Long-term climatological trends driving the recent warming along the Angolan and Namibian coasts”

Folly Serge Tomety¹, Serena Illig^{2,1}, Marek Ostrowski^{1,3}, Founi Mesmin Awo¹,
Marie-Lou Bachèlery⁴, Noel Keenlyside⁴, and Mathieu Rouault¹

¹ Department of Oceanography, Nansen Tutu Center, University of Cape Town, Cape Town, Rondebosch, South Africa.

² Laboratoire d'Etudes en Géophysique et Océanographie Spatiale (LEGOS), CNRS/IRD/UT3/CNES, Toulouse, France

³ Institute of Marine Research and Bjerknes Centre for Climate Research, Bergen, Norway

⁴ Geophysical Institute, University of Bergen and Bjerknes Centre for Climate Research, Bergen, Norway

Manuscript submitted to *Climate Dynamics* in January 2024

Manuscript revised in May 2023

Introduction

This **supplementary material** provides additional figures to compare decadal trend estimated from our composite SST product (see **section 2.1**) to the individual observed SST datasets, namely the weekly and daily Optimum Interpolation satellite-derived SST data (Reynolds *et al.*, 2002; Huang *et al.*, 2021) at $1^\circ \times 1^\circ$ and $0.25^\circ \times 0.25^\circ$ spatial resolution, respectively, and the $1^\circ \times 1^\circ$ Hadley SST data (Rayner *et al.*, 2003).

Fig.S1 shows the map of long-term decadal trend estimated for OISST1, OISST0.25, and HadiSST. They can be compared to the decadal trend estimated from the composite observational product at $1^\circ \times 1^\circ$ resolution shown **Fig.1b**. The three products depict separately the coastal decadal warming trend off Angola of more than $0.2^\circ\text{C}/\text{decade}$ described in the introduction. Notably, the 1° -OISST exhibits a very weak trend in the northern part of the Angola (7°S - 11°S), while the HadiSST shows a decadal cooling trend off central and southern Namibia between 20°S and 25°S , up to $-0.15^\circ\text{C}/\text{decade}$ (in agreement with our CROCO modeling results, see **Fig.3a**). This cooling trend differs from the decadal trend estimation from both OISST products. However, at seasonal scales (see **Fig.S2**), HadiSST also exhibits a warming trend in the austral autumn and summer, in agreement with the OI-SST products and the ocean model results.

Fig.S2 further shows that there is reasonable agreement among the 3 observational products with respect to spatial and seasonal trends. The decadal warming trend during the late austral spring and summer (October-January) is evident in all observational products. However, the agreement decreases during the rest of the year. In particular, the 1° -OISST shows a strong cooling trend in the austral winter north of 10°S , whilst other products (OISST0.25 and

HadiSST) do not. This discrepancy contributes to the overall weaker warming trend observed in the 1°-OISST. Furthermore, in the Namibian region, HadiSST shows a strong cooling trend during the austral autumn, winter and spring, while OISST0.25 shows a much weaker warming trend.

The discrepancies in decadal trends can be attributed to differences in the *in-situ* and satellite data, as well as the gridding strategies used to construct the respective product. While all three products are satellite derived, the limited daily grid coverage requires the use of *in-situ* data and different interpolation techniques by HadiSST, 1°-OISST, and 0.25°-OISST to effectively fill data gaps.

Figures

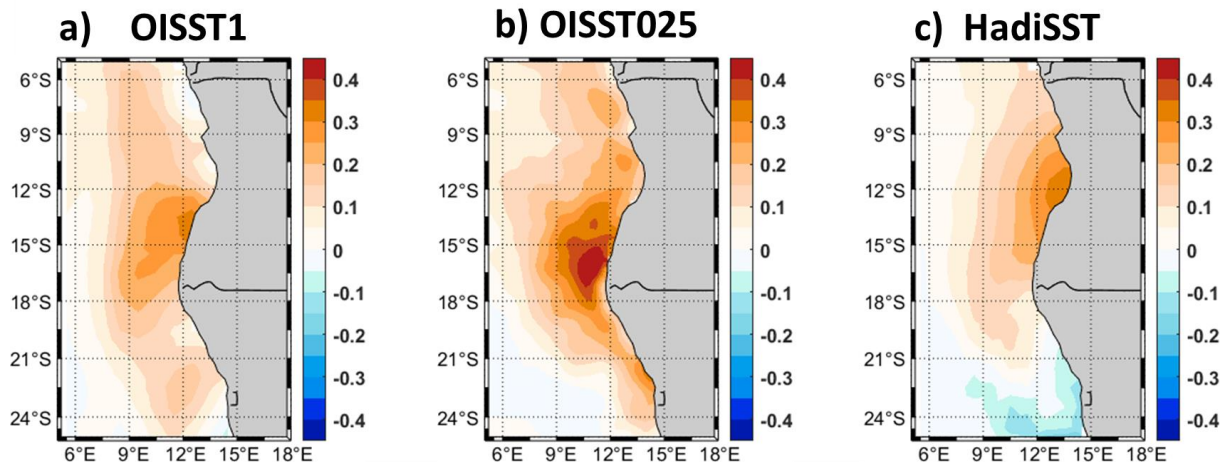


Figure S1: Same as **Fig.1b** for each observational product analyzed on their original resolution. Long-term decadal trend (in °C/decade) from (left) the weekly OI-SST at 1°×1° resolution, (middle) daily OI-SST at 0.25°×0.25° resolution, and (right) Hadley SST at 1°×1° resolution. Individual decadal trend estimates can be compared to the decadal trend computed from the composite observational product (see **Fig.1b**).

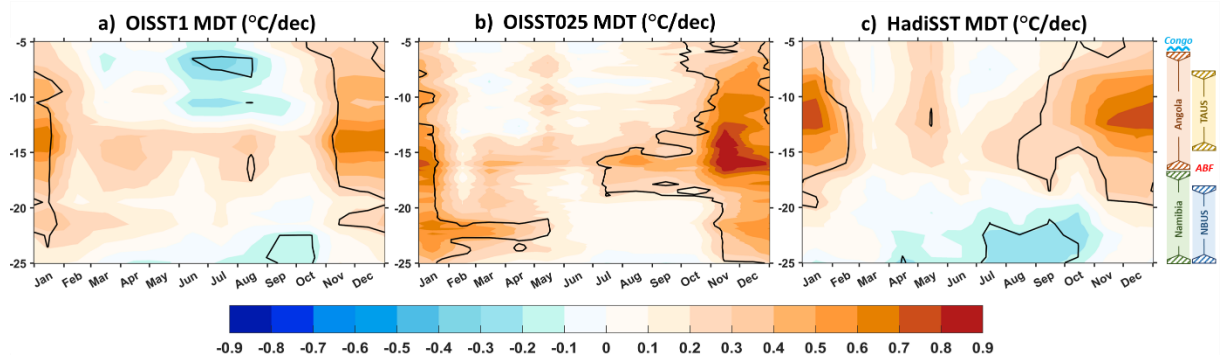


Figure S2: Same as **Fig.3b** for each observational product analyzed individually. Coastal SST Monthly climatological Decadal Trends (MDT, in °C/decade) for (a) the weekly OI-SST at 1°×1° resolution, (b) the daily OI-SST at 0.25°×0.25° resolution, and (c) the Hadley SST at 1°×1° resolution. Dashed contours indicate statistically significant values at the 95% confidence level.

References

- Huang, B., C. Liu, V. Banzon, E. Freeman, G. Graham, B. Hankins, T. Smith, and H.-M. Zhang (2021), Improvements of the daily optimum interpolation sea surface temperature (DOISST) version 2.1, *Journal of Climate*, 34(8), 2923-2939, doi:<https://doi.org/10.1175/JCLI-D-20-0166.1>.
- Rayner, N., D. E. Parker, E. Horton, C. Folland, L. Alexander, D. Rowell, E. Kent, and A. Kaplan (2003), Global analyses of sea surface temperature, sea ice, and night marine air temperature since the late nineteenth century, *Journal of Geophysical Research: Atmospheres*, 108(D14), 4407, doi:<https://doi.org/10.1029/2002JD002670>.
- Reynolds, R. W., N. A. Rayner, T. M. Smith, D. C. Stokes, and W. Wang (2002), An improved in situ and satellite SST analysis for climate, *Journal of climate*, 15(13), 1609-1625, doi:[https://doi.org/10.1175/1520-0442\(2002\)015%3C1609:AIISAS%3E2.0.CO;2](https://doi.org/10.1175/1520-0442(2002)015%3C1609:AIISAS%3E2.0.CO;2).